

TITLE

Significance of Sedimentary Organic Matter Input for Shale Gas Generation Potential of
Mississippian Mudstones, Widmerpool Gulf, UK

AUTHORS & AFFILIATIONS

Sven F. Könitzer (corresponding author)^{a*}

Michael H. Stephenson^b

Sarah J. Davies^a

Christopher H. Vane^b

Melanie J. Leng^{c,d}

^aDepartment of Geology, University of Leicester, University Road, Leicester, LE1 7RH, UK

^bBritish Geological Survey, Keyworth, Nottingham, NG12 5GG, UK

^cNERC Isotope Geoscience Laboratory Facilities, British Geological Survey, Keyworth,
Nottingham, NG12 5GG, UK

^dCentre for Environmental Geochemistry, School of Geography, University of Nottingham,
Nottingham, NG7 2RD, UK

*present address: PanTerra Geoconsultants B.V., Weversbaan 1-3, 2352 BZ Leiderdorp, The
Netherlands, s.koenitzer@panterra.nl, Phone +31(0)715813544

ABSTRACT

Carboniferous mudstones in central and northern England are shale gas prospects but the controls on the amount and composition of organic matter are not well understood, even though these parameters define the volumes of gas generated in fine-grained sediments. Organic matter in samples from basinal late Mississippian (Arnsbergian) mudstones in the Widmerpool Gulf was characterised by using semi-quantitative ($n = 58$) and quantitative palynofacies ($n = 16$) analyses, sporomorph counts and bulk rock geochemistry (total organic carbon, $\delta^{13}\text{C}$ of bulk organic matter, Rock-Eval Pyrolysis).

The results of this study suggest that most organic matter at this location was delivered to the sediment-water interface as aggregates of a granular translucent type of amorphous organic matter (AOM_{Gr} , mean $66.7 \pm 19.3\%$) via hemipelagic suspension settling. AOM_{Gr} represents fragments of algal material with subordinate inclusions of small plant fragments and pyrite framboids held together by microbial colonies. AOM_{Br} (brown granular amorphous organic matter) is the second most abundant group (mean $15.6 \pm 8.5\%$) comprising similar microbial colonies that grew on suspended land plant-derived fragments in the water column. Palynofacies components representing clearly terrestrial organic matter are much less abundant and include gelified organic matter (G, mean $9.6 \pm 12.6\%$), black phytoclasts (Ph_{Bl} mean $2.7 \pm 4.7\%$), brown phytoclasts (Ph_{Br} , mean $3.3 \pm 3.6\%$) and sporomorphs (mean $1.4 \pm 1.3\%$). Sediment delivery processes influence the balance between terrestrial organic matter and AOM_{Gr} . During low sea-level times, turbidity currents and debris flows delivered terrestrial organic matter (representing 12 to 40% of the palynofacies). Kerogen composition varies between Type II and III. In contrast, thin-bedded carbonate-bearing mudstones deposited during rising and high sea-level contain up to 95% AOM_{Gr} and these high abundances correspond to higher total organic carbon. Carbonate and AOM_{Gr} were generated by high bioproductivity in the water column. Type II (oil- and gas-prone) kerogens are dominant in these mudstones and therefore these intervals represent the best potential targets for thermogenic shale gas.

Highlights:

- organic matter assemblages from Namurian mudstones of Derbyshire are described
- two amorphous organic matter (AOM) types are distinguished
- total organic carbon was controlled by bioproductivity
- ratio marine/terrestrial organic matter was controlled by sediment delivery process
- mudstone facies rich in granular amorphous organic matter (AOM_{Gr}) have high gas generation potential

Keywords: source rock, AOM, shale gas, palynofacies, mudstone, sediment delivery processes

1. INTRODUCTION

The hydrocarbon source rock potential of fine-grained sediments is largely controlled by the original amount and composition of sedimentary organic matter buried with the sediment. Understanding small-scale variations of organic matter in relation to sedimentary processes and changes in depositional environment is crucial for identifying prolific source rock intervals, particularly in prospective gas shales (e.g. Passey et al., 2010; Aplin and Macquaker, 2011). This is important because gas concentrations are not evenly spread in shale gas reservoirs, unlike in conventional, buoyancy-driven oil and gas fields where hydrocarbons fill intergranular pore spaces as a homogenous phase across a reservoir (Tissot and Welte, 1984; Mann et al., 1997). Early Namurian (Mississippian) basinal mudstones present in subsurface and outcrop in the Pennine province of Central and Northern England are regarded as potential targets for onshore shale gas exploration (Department of Energy and Climate Change, 2010; Selley, 2012; Roche, 2012). Specifically, the Upper Bowland Shale Formation and Edale Shale Group mudstones are believed to represent source rocks for conventional hydrocarbon finds in this region (e.g. Fraser et al., 1990; Smith et al., 2010); however, detailed studies determining the depositional controls of oil and gas producing intervals are lacking. The re-evaluation as shale gas reservoirs requires refined investigations of the distribution and composition of organic matter (OM) within these mudstone-dominated successions.

In this study, we present organic geochemical and palynological data from mudstones obtained from one fully cored borehole located in the Widmerpool Gulf, Derbyshire, UK. We describe the variability of organic matter present in these mudstones, and relate the OM content to sedimentary processes and changing depositional environment. The findings presented here contribute to current understanding of how biological input affects the shale gas source rock potential of fine-grained sediments.

Previous studies of Mississippian mixed shallow marine to deltaic deposits in the Northumberland Basin and the Alston Block revealed that amorphous organic matter (AOM) and land plant fragments (phytoclads) are the main organic matter constituents and the ratio between these determines the overall characteristics of the bulk OM. Because AOM is dominant in samples from marine limestone horizons (Stephenson et al., 2008) and their equivalent clay-rich marine bands in the Pennine Basin (Hawkins et al., 2013), with mean bulk organic $\delta^{13}\text{C}$ around -28.5‰ (Lewan, 1986), it has been interpreted to originate from marine phytoplanktonic and other algae. In contrast, land-derived phytoclads characterise the terrestrially influenced fluvio-deltaic intervals (Frank and Tyson, 1995; Stephenson et al., 2008). Bulk terrestrial OM can also be distinguished by its average $\delta^{13}\text{C}$ of -23.5‰ (Peters-Kottig et al., 2006). This isotopic pattern has been used in several studies conducted on bulk OM of Carboniferous age (e.g. Maynard, 1981; Wenger et al., 1988; Stephenson et al., 2008; Davies et al., 2012), although absolute $\delta^{13}\text{C}$ levels of these end members vary through this period in response to global changes in atmospheric CO_2 (Stephenson et al., 2010). Similar studies, however, have not been undertaken for the mudstone-dominated successions deposited in the deeper water basins of the southern Pennine province during the early Namurian. Several studies suggest that partly fossiliferous mudstones, including the marine bands contain more total organic carbon (TOC) than fossil-barren intervening mudstones (e.g. Spears and Amin, 1981; Kombrink, 2008; Smith et al., 2010); however no specific links between sedimentary processes and depositional environment with OM content and composition have been reported.

Here we use a detailed palynofacies scheme (Table 1) to track changes in the composition of particulate OM through a vertical borehole section. The relative abundance of the palynofacies groups, obtained from point counts, is compared with bulk total organic carbon, organic $\delta^{13}\text{C}$ and microlithofacies data compiled in Könitzer et al. (2014). Thus we examine the variation of organic matter content with respect to sediment delivery processes and depositional environment. This

study also represents one of the first transmitted light microscopic investigations of Carboniferous organic matter attempting to distinguish different types of AOM and to critically consider the possible origin and processes of these types. Finally, we discuss the hydrocarbon source rock properties, obtained from Rock-Eval parameters, for all lithofacies and OM types present.

2. GEOLOGICAL SETTING

The Widmerpool Gulf is one of several small, linked marine basins in the southern Pennine province which acted as depocentres for fine-grained sediments of the Edale Shale Group during the Visean to Namurian. This area was located between the northern Pennine province which was influenced by regional supply of siliciclastic material from fluvio-deltaic systems from the north-east (Collinson, 1988; Waters and Davies, 2006) and the emergent Wales-London-Brabant High in the south (Fig. 1). Sedimentation in the basins was characterised by the accumulation of dark, fissile mudstones in a continuously submerged setting in water depths of a few hundred metres (Collinson, 1988; Aitkenhead et al., 2002). Significant rises in sea-level are recorded by (in places) fossiliferous mudstone successions. These include 'marine bands', intervals which contain diagnostic ammonoid fauna used for biostratigraphic subdivision and correlation (Ramsbottom, 1977; Holdsworth and Collinson, 1988; Davies, 2008) and are interpreted as maximum flooding surfaces (e.g. Hampson et al., 1997). During sea-level regressions, mudstones barren of macrofossils were deposited with interbedded silt- and sandstone turbidites delivered from delta slopes fringing the Wales-London-Brabant High (Trewin and Holdsworth, 1973; Aitkenhead, 1977; Chisholm et al., 1988; Collinson, 1988).

Sea-level fluctuations are thought to have been driven by glacio-eustatic forcing (Ramsbottom, 1977; Holdsworth and Collinson, 1988; Hampson et al., 1997; Stephenson et al., 2010; Waters and Condon, 2012). The first glacial phase C1 of significant ice sheets in the southern hemisphere during the late Pendleian to mid-Arnbergian (Fielding et al., 2008) induced high-frequency and high-magnitude sea-level fluctuations following c. 110 ka and 400 ka Milankovitch eccentricity

rhythms (Waters and Condon, 2012). The E_{2a3} (*E. yatesae*) marine band present in the studied succession (Fig. 1C) is considered to represent one of the major, 400 ka flooding events during C1 (Waters and Condon, 2012).

The Namurian Pennine province was characterised by a humid equatorial climate with seasonally drier intervals (Davies, 2008). Low-lying land areas, particularly fluvio-deltaic plains, were consequently covered by dense wetland forests that contracted and expanded in response to transgressions and regressions respectively (Neves, 1958; Turner et al., 1994; Davies and McLean, 1996; Falcon-Lang, 2004). Floral communities reconstructed for Pennsylvanian vegetational belts (e.g. Scott, 1979; Falcon-Lang et al., 2006) are thought to comprise lycospid trees and shrubs, ferns, putative pteridosperms and early cordaitaleans. Broadly similar spore assemblages characterise the early Namurian (latest Mississippian) palynostratigraphic record (e.g. Stephenson et al., 2008), suggesting that plant evolutionary trends established at Devonian-Mississippian times persisted into the Pennsylvanian (Traverse, 1988). The typical floral communities of the late Mississippian to early Pennsylvanian likely also occupied the late Mississippian alluvial and deltaic areas of the Wales-London-Brabant High that supplied most of the terrestrial debris.

2.1. Studied section

Core material from the Carsington Dam Reconstruction C4 well [SK 244 503] records a succession of E_{2b} (middle Arnsbergian) to E_{2a2} (late early Arnsbergian) age from depths of 14.00 m to 55.50 m (Fig. 1C). Below 33.85 m an interbedded sequence comprising clay-rich mudstones and millimetre- to centimetre-scale, commonly graded silt-rich mudstones and sand-bearing siltstones occur. Many siliciclastic beds exhibit plant fragments either at their irregular bases or in layers within their tops and individual leaf or thin woody fragments are also found in the clay-rich mudstones. In the overlying succession, above 33.85 m, silt-rich beds are absent; and carbonate-bearing mudstones dominate with only minor silt content and rare individual plant fragments.

Posidonia corrugata and other calcareous fossils can be found sporadically to commonly throughout this interval (in accordance with Aitkenhead, 1991), indicating deposition under fully marine conditions. The *Eumorphoceras yatesae* (E_{2a3}) and *Cravenoceratoides edalensis* (E_{2b}) marine bands were placed within the top unit (Aitkenhead, 1991), although ammonoids (mainly *Ct. edalensis*) occur at several depths and these biostratigraphic markers represent a zone rather than a discrete horizon. Carbonate-bearing mudstones with bivalves occur between 52.60 m and 53.10 m. This interval may represent one of two fossiliferous intervals of the *Cravenoceras gressinghamense* (E_{2a2α}) marine band introduced by Brandon et al. (1995), and as such possibly indicate an earlier marine transgression.

2.2. Lithofacies characteristics

Seven different microlithofacies, that were introduced by Könitzer et al. (2014), are present in the Carsington section (Fig. 2).

Four of the facies represent more distal locations, with limited sediment input by density currents. These include the clay-rich carbonate-bearing mudstones (Facies 1; average TOC=4.6±1.3%; n=26) and calcareous mudstones (Facies 2; TOC=0.3%; n=2) were deposited under high biologic productivity (both organic and carbonate production) in distal locations beyond the influence of sediment density currents. Lenticular clay-dominated mudstones (Facies 3; TOC=3.0±0.9; n=9) and thin-bedded silt-bearing clay-rich mudstones (Facies 4) also represent relatively distal locations, but record slightly lower bioproductivity. Three subfacies of Facies 4 are distinguished: lenticular (Facies 4a; TOC=2.4±0.6%; n=7), homogeneous/burrowed (Facies 4b; TOC=2.0±0.6%; n=15) and organic-rich (Facies 4c; TOC=3.7% and 3.4%; n=2).

The three remaining facies accumulated during periods of low sea-level, when distal turbulent flows and more energetic turbidity currents reached the site of deposition. These include thick-bedded graded silt-bearing mudstones (Facies 5; TOC=1.7±0.3%; n=6), sand-bearing silt-rich

mudstones (Facies 6; TOC=1.8±0.9%; n=5) and plant debris- and sand-bearing mudstones (Facies 7; TOC=9.7% and 7.1%; n=2).

3. METHODS

In total, 110 whole rock samples covering the entire Carsington Dam Reconstruction C4 core section (Fig. 1) were processed for $\delta^{13}\text{C}$ analyses. From 58 out of the 110 samples (listed in Table 3), around 5 g of material were extracted for palynofacies, of which 16 were processed for quantitative palynology.

All 110 samples were crushed and milled, and carbonate was removed during acidification with 10% HCl (see Könitzer et al., 2012 for protocol). Two samples may contain traces of siderite (samples 23 and 25), and another two contain dolomite (samples 33 and 34), neither of which could be removed. Contamination by potential migrated hydrocarbons, which would deplete bulk $\delta^{13}\text{C}$ values (Stephenson et al., 2005), was excluded (see Könitzer et al., 2012) so bitumen was not extracted. For analysis, a measured amount of 5 to 100 mg of each sample was filled into tin capsules, which were subsequently squashed. The amount of carbon (%C) and the $\delta^{13}\text{C}$ composition of the decarbonated residue were determined by combustion in a Costech ECS4010 elemental analyser (EA). Based on results of the studies above, we regard %C as per cent total organic carbon (TOC) and $\delta^{13}\text{C}$ as $\delta^{13}\text{C}_{\text{org}}$. The decarbonated residues from 32 of 110 samples were used for Rock-Eval Pyrolysis.

Vitrinite reflectance (R_0) at Carsington is $\leq 0.6\%$ (Smith et al., 2010), suggesting that the OM is thermally immature or in the low range for oil generation (oil window for type II kerogen typically ranges from 0.5 to 1.2%). Therefore we do not expect thermal maturation effects on bulk $\delta^{13}\text{C}$, particulate OM, or Rock-Eval parameters.

3.1. *Palynological processing and palynofacies counts*

All palynological slides were prepared at the British Geological Survey using standard techniques (Wood et al., 1996) involving HCl (36%) and HF treatments (40%) of whole rock subsamples. The residues (kerogen) were sieved using a 10 µm mesh and washed with distilled water before they were mounted onto cover slips, adding one drop of PVA and mounted onto slides using Elvacite. An oxidation step was not conducted.

Initial observation of the palynological assemblages under white and incident UV light was undertaken with a Zeiss microscope fitted with a UV lamp and an AxioCam MRc 5 camera. Based on these observations, a classification scheme for the different palynofacies components was developed (Table 1). Palynofacies composition data was produced using a Leitz Aristoplan microscope and an electrical point counter. Point counting is rarely employed in optical studies of OM (with the exception of for example Ando et al., 2003); however, this technique provides a more accurate approximation of the composition of OM compared to conventional estimates based on the number of OM particles (Powell et al., 1982). This is because counts of one particle in the centre of the field of view are taken in regular intervals, and the probability of a component being counted depends on its areal proportion within the assemblage (particle frequency and size), rather than just the number of particles present. In addition, as only one count is taken per field of view, the areal coverage of the slides is increased (Tyson, 1995). For each sample 500 counts were taken along non-overlapping traverses. According to Traverse (1988), a category constituting 5% of the total assemblage will have a standard deviation of 20% (i.e. $5 \pm 1\%$), while a category representing 1% will have a standard deviation of 40% (i.e. $1 \pm 0.4\%$). This reproducibility is deemed acceptable for the present study because proportions of significant (i.e. around 10% or greater) palynofacies groups can be compared. Small differences in proportions of rare groups (below 10%) are more problematic to interpret; however, the standard deviation of these groups would not significantly improve if a higher count size was used (Traverse, 1988).

In addition, 16 of these samples were prepared quantitatively, i.e. a measured amount of rock sample (c. 5 g) was processed as outlined above. The residue was diluted with distilled water in a centrifuge tube to 10 ml, homogenised, and a measured aliquot of 0.10 ml was transferred onto a cover slip and then onto a slide. Due to the abundance of organic matter in most samples, the aliquot was spread on three to five slides. The most appropriate slide of each sample preparation were used for palynofacies counts, but also to determine the concentration of sporomorphs (terrestrial spores and pollen) per g of sediment, which were obtained by counting all sporomorphs in non-overlapping traverses across the entire slide. The concentration of sporomorphs (C_S) was used to convert the proportion of each palynofacies category into equivalent (eq) concentrations (C_i) as follows:

$$C_i \left[\frac{\text{particles}}{g} \text{ eq} \right] = C_S \left[\frac{\text{sporomorphs}}{g} \right] \times \frac{P_i [\%]}{P_S [\%]} \quad (\text{Equation 1})$$

where P_i is the proportion of the individual palynofacies category and P_S is the proportion of sporomorphs, both derived from point counting data.

The total yield of organic matter (C_{total}) is derived from:

$$C_{\text{total}} \left[\frac{\text{particles}}{g} \text{ eq} \right] = \sum_{i=AOM_{Gr}, AOM_{Br}, G, Ph_{Bl}, Ph_{Br}, A} C_i \left[\frac{\text{particles}}{g} \text{ eq} \right] + C_S \left[\frac{\text{sporomorphs}}{g} \right] \quad (\text{Equation 2})$$

Concentrations per g of rock, rather than proportions of an assemblage, provide independent control on the absolute abundance of a palynofacies category, i.e. a rise or decrease in one category will not necessarily result in an apparent decrease or increase in another. Due to the relative scarcity of sporomorphs (resulting in a high standard deviation), however, the calculated yields of other palynofacies groups have considerable uncertainty. If the method was accurate, we expect that variations in the total yield of organic matter (Equation 2) would be broadly

concordant with TOC changes. A plot showing the correlation of these parameters is shown in Figure 11.

The recorded sporomorphs were divided into ecological groups (Table 2) following the classification by Stephenson et al. (2008), based on Davies and McLean (1996).

3.2. Carbon isotope measurements of organic fractions

In addition to $\delta^{13}\text{C}$ analyses of bulk OM ($\delta^{13}\text{C}_{\text{org}}$), 6 organic residues from palynological slide preparation were processed to obtain approximate $\delta^{13}\text{C}$ values of isolated AOM ($\delta^{13}\text{C}_{\text{AOM}}$). The selected residues, all of which are dominated by AOM, were sieved using distilled water and metallic meshes at 106 μm , 180 μm , 250 μm , 300 μm and 350 μm , in order to exclude small ligneous debris (<100 μm) and/or larger plant fragments. The size fractions were visually inspected under a microscope by pipetting a drop of the solution onto a cover slide. The $\delta^{13}\text{C}$ data were obtained following the same procedure as for bulk samples. Samples were filled as a solution with distilled water into tin capsules, and the water was evaporated. The results are shown in Table 4.

For the $\delta^{13}\text{C}$ measurement of isolated land plant material ($\delta^{13}\text{C}_{\text{wood}}$), samples of macroscopic woody or leaf material were collected from the core where present. The results of these measurements are included in Table 4.

3.3. Rock-Eval Pyrolysis

Pyrolysis was performed on approximately 60 mg (dry/ wt) of sample powder using a Rock-Eval 6 analyser (Vinci Technologies) in standard configuration (pyrolysis and oxidation as a serial process). Samples were heated from 300°C (hold 3 min) to 650°C (hold 3 min) at 25°C/min in an inert nitrogen atmosphere. The residual carbon was then oxidised at 300°C to 850°C at 20°C/min (hold 5 min). Hydrocarbons (HC) released during the two stage pyrolysis were measured using a flame ionisation detector (FID). The CO and CO₂ released during thermal cracking of the bound OM were monitored using an IR cell. The performance of the instrument was checked every 10

samples against the accepted values of Institut Français du Pétrole (IFP) standard (IFP 160000, S/N1 5-081840). Standard Rock-Eval parameters (Table 7) were calculated by integration of the amounts of HC: thermo-vaporised free hydrocarbons expressed in mg HC/g rock (S1) and hydrocarbons released from cracking of bound OM expressed in mg HC/g rock (S2) as well as CO and CO₂. T_{max} was calculated from $T_{pS2} - \Delta T_{max}$, where T_{pS2} is the temperature at which maximum release of HC occurs (the top of the S2 peak) and ΔT_{max} is the difference between T_{pS2} of the IFP standard and its accepted T_{max} (419 °C). Production Index (PI) is calculated from $S1/(S1+S2)$, Hydrogen Index (HI) is calculated from $S2 \cdot 100/TOC$, and Oxygen Index (OI) is derived from $S3 \cdot 100/TOC$, where S3 is the amount of CO₂ produced from the organic matter.

It should be noted that TOC values derived from Rock-Eval are consistently lower (by $34.5 \pm 9.9\%$ on average, $R^2=0.91$) than those from the elemental analyser (compare Table 3 and Table 7). In a comparative study, Disnar et al. (2003) found the same relationship in TOC between Rock-Eval and a Leco analyser, although the difference was smaller. This offset was attributed to a lower response of the FID to less hydrogen-rich pyrolysates than to those of the IFP standard, and to the loss of hydrogen consumed during hydration reactions. The underlying causes of the larger offset in this study are uncertain, however, we will be referring to TOC values determined by the elemental analyser due to the larger encompassing dataset, except for results relating to Rock-Eval characteristics. It should also be noted that for Rock-Eval, the two calcareous samples of Facies 2 were not corrected for the loss of weight during decarbonating. This does not affect HI and OI data of the samples, but TOC and S1-S3 data (Fig 11b) are in fact much lower than the Rock-Eval data suggests.

4. RESULTS

4.1. *Palynofacies composition*

The palynofacies assemblages show a variety of structureless (amorphous or gelified) to structured (phytoclads, algae remains and sporomorphs) organic constituents (Table 1). Granular translucent amorphous (AOM_{Gr}) particles are most common. These particles have irregular, diffuse outlines and occur as coherent masses ranging from translucent to pale brown or dark grey in different sizes (Plate I). Inclusions of various sizes (brown to black opaque, sometimes elongate, fragments and/or pyrite) create a fine or coarse granular appearance of the particles. They are characterised by moderate to strong irregular, patchy fluorescence (Plate III).

Particles with morphologic properties of both AOM_{Gr} and phytoclads can be observed which are labelled brown granular amorphous OM (AOM_{Br}). Typical AOM_{Br} particles contain an inner structureless, opaque zone surrounded by a more or less extensive granular amorphous margin with the same optical properties as AOM_{Gr} (Plate I); however under ultraviolet light they show the same fluorescence properties as AOM_{Gr} (Plate III-2). Less commonly, AOM_{Br} may also include granular amorphous particles overgrowing fragments with a relict biostructure (Plate I-4).

Gelified OM (G) particles, in contrast, are massive, brown to black opaque, lustrous and have a better-defined outline (Plate II-1). Particles are present in the full size range of the organic residue (10 – 500 μm). They also exhibit weak, but more homogenous fluorescence, which might be slightly higher around the edges. Vitrinites (angular, homogenous brown to gradually black particles with sharp edges; Plate II-2) are included in gelified OM (cf. Combaz, 1980).

The main category of structured material comprises phytoclads which are fragments showing vascular or cuticular characteristics of land plants (Tyson, 1995). Detectable particles (for point counts) are commonly between 20 μm and 500 μm (but rarely over 300 μm), while smaller fragments tend to be present as inclusions within AOM_{Gr} particles (Plate I-5). Brown phytoclads (Ph_{Br}) are light or dark brown, translucent lath-shaped fragments with regular structures, such as

perforated cross-hatching, pits or elongated cells (Plate II-4). They may show weak fluorescence (Plate III-4). Black phytoclasts (Ph_{Bl}) have similar sizes as brown phytoclasts, but are distinguished by their colour, opacity, and their slightly more angular, commonly elongated shape (Plate II-3). Their outlines may resemble those of brown phytoclasts, but more commonly they also show signs of abrasion, for example holes and cavities (Tyson, 1995). Black phytoclasts are non-fluorescent (Plate III).

Observed sporomorphs (S) include circular to triangular spores (up to 100 μm) and larger (100 – 300 μm) monosaccate pollen. These entities exhibit high to very high fluorescence (Plate III-3, 4). Algal remains (A) are represented by translucent to yellow-grey tubes or filaments (Venkatachala, 1981; Plate II-5, 6). Thin, translucent-yellow and circular sheets are interpreted as algal phycoma (mainly Leiospheres; Tyson, 1987, Stephenson et al., 2004). However, often these particles are inconspicuous and difficult to visually separate from translucent amorphous particles. Spinose forms, such as acritarchs, are more distinct but too rare to be of importance. Under incident ultraviolet light, algae remains are easier to distinguish due to their intense orange to yellow fluorescence (Plate III-1). Individual particles of resin and fungal remains were only encountered in a few samples and are not included in the scheme.

4.2. *Palynofacies Assemblage Trends*

In virtually all 58 samples AOM_{Gr} is the main palynofacies group (mean= $66.7\pm 19.3\%$). Only 6 samples, all located below 33.85 m, contain $<50\%$ AOM_{Gr} (Fig. 3). In the top section above 33.85 m AOM_{Gr} is the major to dominant particle group (range 55.5–95.2%). AOM_{Br} is the second most abundant group (mean= $15.6\pm 8.5\%$), and is present in proportions between 10 and 20% in most samples. Abundance variations of this group do not appear to be systematic and are not linked to certain depth intervals or facies.

Given this overwhelming presence of the two AOM types, significant relative contributions (i.e. $>10\%$) of other categories are found only in a couple of samples exclusively located in the basal

section below 33.85 m. Gelified OM (mean=9.6±12.6%) is typically below 10%, and only 2 samples have more than 20% (sample 49: 80.4% and sample 43: 40.2%). Black and brown phytoclasts (Ph_{Bl}, Ph_{Br}) are less abundant (mean=2.7±4.7% and 3.3±3.6% respectively) compared with gelified OM, but have similar distributions. Above 33.85 m, contributions from the combined phytoclast groups are typically <5%. The ratio between black opaque phytoclasts and biostructured brown phytoclasts remains broadly constant throughout. Sporomorphs are a comparatively rare category (mean=1.4±1.3%). Their distribution is similar to phytoclasts and gelified OM, with episodic peaks (up to 30 counts, or 6%; Fig. 3) within the basal unit, and reduced abundance in the top unit (above 33.85 m). Definite algal remains (A) such as cysts (Plate III-1) or prasinophytes are very rare (0.5±1.1%) and are absent in 13 samples. The mean palynofacies assemblages in each lithofacies are summarised in Table 5 and shown in Figure 4. The relative abundances of AOM_{Gr} against gelified OM plus total phytoclasts display an approximate correlation with the $\delta^{13}\text{C}_{\text{org}}$ composition of the bulk OM (Fig. 9). Increasing proportions of AOM_{Gr} are associated with more negative $\delta^{13}\text{C}_{\text{org}}$ ($\leq -28.0\text{‰}$; $R^2=0.65$). Consequently, inverse trends can be observed between $\delta^{13}\text{C}_{\text{org}}$ and the proportion of phytoclasts plus gelified OM.

The strata below 33.85 m in the Carsington core are characterised by two different typical OM compositions. Despite different sedimentary attributes, the clay-dominated (Facies 3, lenticular) and thin-bedded silt-bearing clay-rich mudstones (Facies 4a, lenticular and 4b, homogenous and/or burrowed) are characterised by high average AOM_{Gr} proportions, subordinate percentages of AOM_{Br} and minor fractions of land-derived material (Fig. 4). Facies 4a and 4b exhibit only slightly higher phytoclast proportions compared with Facies 3. The sample of Facies 4c is enriched in gelified OM and phytoclasts and has lower AOM_{Gr} proportions. In contrast to the AOM_{Gr}-rich assemblage found in Facies 3, 4a and 4b, the thicker-bedded silt-bearing (Facies 5) and sand-bearing silt-rich (Facies 6) mudstones, while being relatively OM-poor, contain significant contributions of gelified material and phytoclasts, and moderate AOM_{Gr} percentages,

concordant with relatively high $\delta^{13}\text{C}_{\text{org}}$ values. Facies 5 also contains the highest average proportions of both phytoclasts and sporomorphs, whereas Facies 6 is particularly rich in gelified OM. The sample of Facies 7 is characterised by the predominant occurrence of gelified OM with few AOM_{Br} , AOM_{Gr} and phytoclast particles.

Above 33.85 m, the mainly thin-bedded carbonate-bearing mudstones (Facies 1), with subordinate lenticular clay-dominated mudstones (Facies 3) and two thin calcareous mudstones (Facies 2) are dominated by AOM_{Gr} with relatively minor terrestrial contributions. Absolute concentrations of AOM_{Gr} and, to a lesser extent, of AOM_{Br} are considerably higher compared with the basal section, and this is consistent with higher TOC. AOM_{Br} is also a significant component in some samples in association with slightly higher gelified OM and phytoclast proportions. Similar abundances of plant material and sporomorphs to those characterising the basal section are observed in a one or two samples (Fig. 3).

4.3. *Quantitative Palynofacies*

Yields of sporomorphs, directly derived from counts of spores and pollen, vary between 20,000 and 280,000 specimen/g of rock (Fig. 5). The highest concentrations tend to be present in Facies 4c and 5 (but not in Facies 6) within the basal section, and relatively lower concentrations (up to 100,000/g) occur within the top section.

The total yield of organic matter (derived from Equation 2) is not consistently correlated with TOC content (Fig. 6). Some increases in TOC are associated with an increase in the total yield of organic matter particles, but some are associated with a decrease in organic matter yields. For example, sample 23 has a high total yield comparable to that of sample 106 (Table 6); however the TOC content is only half (2.1 and 4.5% respectively). As a result, the quantitative palynofacies results have limited significance. The concentrations of AOM_{Gr} are highest within the top section, with maximum values in Facies 3 (around 8×10^6 particles/g eq), although this facies has slightly less TOC than Facies 1. AOM_{Gr} concentrations within Facies 1 tend to decrease upwards from

8×10^6 particles/g eq to values between 3×10^6 and 5×10^6 particles/g eq. Facies 4b and 4c (2.7×10^6 particles/g eq), 5 and 6 (0.8×10^6 particles/g eq) have lower content of AOM_{Gr} . AOM_{Br} is abundant in some samples in the top unit (up to 3.3×10^6 particles/g eq) and low in the basal unit except in one sample of Facies 5. The concentration of gelified OM is up to 1.2×10^6 particles/g eq in Facies 5, and similar values are reached in Facies 4c, 6, but also in some samples of Facies 1 towards the top of the section. A similar distribution, with maximum values of 0.6×10^6 particles/g eq, is observed for total phytoclasts. Abundances of algal remains of less than 100,000 particles/g eq occur in the top section, with minor amounts, if present at all, in the basal section.

4.4. Sporomorph trends

Overall spore and pollen preservation is poor; approximately 50% of sporomorphs are not recognisable due to degradation or deformation caused by pyrite overgrowth. Particularly in the top section, many spores are also partly or wholly occluded by amorphous particles. Out of the sporomorphs identifiable to genus level (Plate IV), *Lycospora* is most abundant (51%). *Lycospora* and *Densosporites* (6%) dominate the forest mire group, while *Granulatisporites* (7%) and *Leiotriletes* (9%) are the most common sporomorphs of the non-forest mire. Less abundant genera include *Punctatisporites* (4%), *Lophotriletes* (3%), *Verrucosisporites* (2%), *Convolutispora* (2%) and *Calamospora* (1%). The colonisers group, represented by *Crassispora*, is rare (1%). Monosaccate pollen, mainly *Florinites* derived from cordaitaleans, constitute 3% of the sporomorph assemblage.

The general upward decline in the abundance of total sporomorphs is reflected by decreasing numbers of all ecological groups, and is most closely mirrored by the non-forest mire group (Fig. 7). The forest mire shows the most dramatic decline, being the main group below 33.85 m and less abundant than non-forest mire in some samples towards the top. In comparison, the proportionate decreases in sporomorphs of colonisers and monosaccate pollen are less pronounced (Fig. 8).

Diversity (the number of sporomorph genera recorded per sample) also shows an upward-decreasing trend, and is opposite to the trend observed in the relative abundance of monosaccates.

4.5. *Rock-Eval Pyrolysis*

Hydrogen indices of the 32 pyrolysates vary between 500 and 100 mg/g TOC (Table 7) and oxygen indices are generally below 50 mg/g. High (>300 mg/g) values, which are characteristic of type II kerogen, are produced by Facies 1, 2, 4a, one sample of Facies 3 and, surprisingly, by the Facies 7 sample (Fig. 10). Facies 4b, 4c, 6 and one sample from Facies 3 exhibit lower hydrogen indices, displaying more typical values of mixtures of type II and III. Facies 5, and one sample from each Facies 4b and Facies 6 can be classified as type III kerogen.

A positive relationship between the relative amount of AOM_{Gr} and hydrogen index is observed (Fig. 11a), reflecting trends seen in the van Krevelen diagram and palynofacies data. The samples which show affinity to type II kerogen (Facies 1, 2 and 3) typically have more than 75% AOM_{Gr} , whereas samples with lower AOM_{Gr} proportions tend to exhibit smaller hydrogen indices.

The S2-TOC plot (Fig. 11b) shows a low-angle linear trend. This shows that samples with increasing TOC comprise gradually more abundant hydrogen-rich components, resulting in higher S2 values (up to 20 mg HC/g of rock).

In accordance with vitrinite reflectance data from Smith et al. (2010), low S1 and T_{max} values and the strong fluorescence displayed by palynomorphs show that the OM in the section is thermally immature for hydrocarbon generation. Therefore we assume that the remaining oil and gas generation potential is fully dependent on the depositional OM content (loss of OM through conversion into hydrocarbons is excluded) and free of thermal maturity effects.

5. DISCUSSION

5.1. *Origin and sources of organic matter*

With few exceptions, the AOM group is the major component of organic material in this section suggesting deposition in a marine environment distant from terrigenous supply routes (Tyson, 1995). AOM has commonly been regarded to derive from degraded marine phytoplankton and bacteria, preferentially under dysoxic or anoxic conditions (e.g. Tissot and Welte, 1984; Jones, 1987; Tyson, 1987; Ercegovac and Kostić, 2006). However, AOM may be formed in non-marine environments (Wood et al., 2002; Paction et al., 2011) and may result from the degradation of plant material (Masran and Pocock, 1981; Batten, 1983; Hart, 1986; Gregory et al., 1991; Tyson, 1995). Two different types of AOM are observed in palynological slides from Carsington. AOM_{Gr} is the major palynofacies group associated with marine macrofauna in this section. Particles of similar appearance as the translucent, and diffuse-edged AOM_{Gr} have been linked to marine phytoplankton (e.g. Venkatachala, 1981; Batten, 1983; Lewan, 1986). Although the overall moderate to strong fluorescence intensity of the AOM_{Gr} particles could suggest algal material (cf. Gregory et al., 1991); the patchy, heterogeneous fluorescence reflects the presence of finely comminuted organic matter constituents. Measurements on the organic residue size fractions dominated by AOM_{Gr} (mean $\delta^{13}\text{C}_{\text{org}} = -28.5 \pm 0.5\text{‰}$; Table 4) are similar to values (-28.5‰) reported for Carboniferous AOM by Lewan (1986). These values suggest a distinct source of organic carbon compared with land plant material (mean $\delta^{13}\text{C}_{\text{org}} = -25.8 \pm 1.0\text{‰}$).

The second type, AOM_{Br}, is similar to AOM_{Gr} with diffuse edges and comparable fluorescence. These characteristics of AOM_{Br} suggest a genetic relationship with AOM_{Gr} but others (e.g. relict biostructure) suggest particles may be plant-derived. Differences in their stratigraphic distribution may be significant: in contrast to AOM_{Gr}, changes in the proportion of AOM_{Br} do not vary systematically, do not follow the $\delta^{13}\text{C}_{\text{org}}$ of the bulk OM and do not appear to be related to certain lithofacies (Fig. 3).

Based on the evidence presented above, we consider that AOM_{Gr} is composed chiefly of marine algal-derived material from the water column. Recent studies (Boussafir et al., 1995; Pacton et al., 2011) have shown that microbial reworking of organic matter in the water column or near the sediment-water interface plays a key role in the formation of AOM. The occurrence of a granular and a gelified AOM type was explained by Pacton et al. (2011) to represent direct microbial products (strong fluorescence) and microbial colonisation of terrestrial fragments respectively. Considering these findings, both AOM types are likely to contain significant proportions of microbes. Microbes likely colonise different organic fragments in the water column, depending on availability. They also bind OM particles together through the production of mucopolysaccharides, thus forming flocs of amorphous OM with mineral grains (Eisma, 1986). AOM_{Gr} probably represents agglomerations of fragments of algal material with subordinate inclusions of small plant fragments and pyrite framboids held together by microbial colonies. AOM_{Br} likely comprises similar microbial agglomerations but growing on suspended land plant-derived fragments in the water column. AOM_{Br} is therefore probably not exclusively marine in origin. The indistinguishable, patchy fluorescence of both AOM types under incident UV light is attributed to the granular amorphous coating present at the surface of AOM_{Br} particles, as incident UV light has little penetrative power (Tyson, 1995).

The discrete gelified OM particles (G) have features in common with phytoclasts, including clear outlines and equant- or lath-like shapes, and particles of similar appearance have been described as degraded phytoclasts by Schiøler et al. (2010). It is known that gelified material can be derived from the diagenetic alteration of plant tissue through hydrolysing reactions (e.g. Combaz, 1980) and the low level fluorescence is also consistent with woody tissue of land plant origin. Significant quantities of gelified organic material are generally more common in samples from the silt-bearing lithofacies, and occur preferentially in samples with phytoclasts (plant fragments), indicating similar provenance. The recognisable biostructure of phytoclasts and sporomorphs are the most conspicuous palynofacies groups of unequivocal land plant origin. Black opaque phytoclasts

(Ph_B) are an important group of vascular plant fragments, because they are interpreted as oxidised or charcoalsed particles, and are more refractory to decomposition (e.g. Batten, 1996; Stephenson et al., 2008), although cuticles are comparatively resistant to physical and chemical degradation (Tyson, 1995).

The gelified OM particles, phytoclasts and sporomorphs are interpreted to represent the terrestrial input of OM. These groups are characterised by several peaks in abundance within the basal interval, whereas their total contribution above 33.85 m is minimal, although these particles, in particular the gelified OM, are still present.

Algae remains, acritarchs and prasinophyte phycoma (A) are very rare in the sample material, except in one calcareous mudstone sample (8.5% at 18.18 m). Although limited numbers of marine phytoplankton are generally recorded in Carboniferous successions, a phenomenon termed the 'Late Palaeozoic phytoplankton blackout' (Riegel, 2008), this scarcity may also relate to the local setting. The confined deeper basin setting (Collinson, 1988) of the Widmerpool Gulf with limited marginal shelf areas might not have been ideal for the production of cysts with a high preservation potential. Accurate proportions of the primary input of algae are uncertain because the overwhelming majority of algal material was likely degraded and transformed into AOM_{Gr} in the water column.

The $\delta^{13}\text{C}_{\text{org}}$ composition of the bulk organic matter (Figure 9) appears to be most sensitive to the proportion of AOM_{Gr} and plant material (G+Ph_{total}). These trends indicate that the ratio of marine-sourced (AOM_{Gr}) to terrestrial-sourced (G+Ph_{total}) components controls $\delta^{13}\text{C}_{\text{org}}$.

5.2. *Processes of organic matter input*

The strata below 33.85 m in the Carsington core were deposited during relative sea-level lowstands (e.g. Ramsbottom, 1977; Holdsworth and Collinson, 1988). Two different typical OM compositions characterise this part of the section:

I - The palynofacies composition of Facies 3 and 4 suggests that deposition of marine-derived OM from the water column was dominant. Input of terrestrially derived OM is subordinate, despite evidence for transport of mud clasts, in Facies 3, and sediment gravity flows in Facies 4a and 4b (Könitzer et al. 2014). AOM_{Gr} (formed of mainly algal remains with microbial colonies) and AOM_{Br} (microbial colonisation of plant fragments) particles were likely delivered as part of flocs associated with clay and fine silt to the sediment-water interface. The hemipelagic settling of flocculated mineral and organic matter was a continuous depositional process but the unconsolidated sediment on the sea bed was frequently reworked by erosive currents, creating water-rich mud clasts that were re-deposited with clay- and organic-rich material after the current had waned. The lower TOC and slightly lower proportions of AOM_{Gr} in the homogenous-bioturbated mudstones (Facies 4b) are attributed to the bioturbating activity of benthic microfauna, whereby the resulting increased ventilation of the top layer of sediment allowed diffusion of oxidants into pore waters. As AOM of marine origin is most degradable (e.g. Tyson, 1987; Ercegovac and Kostić, 2006), it is preferentially oxidised (Whitaker et al., 1992) and therefore slightly reduced in the organic assemblage.

Lower TOC with only marginally higher proportions of Ph_{Br} in Facies 4a and 4b compared to Facies 3, suggest that the silt content supplied by dilute turbidity flows primarily dilutes the OM of the bulk sample without significantly altering its composition. The flows, from which the silt beds are deposited, probably did not originate from near-shore settings; instead they chiefly carried re-suspended silt from the most distal shelf - basin slope. As a result, the suspensions were impoverished in organic matter, compared with the clay-rich interbeds, and transported only few OM fragments. Facies 4c, however, were deposited from flows transporting abundant land-derived material.

II - The cm-scale beds and abundance of silt- and fine sand-grade material suggest that Facies 5 and 6 were derived from distal, yet more energetic, higher density-turbidity flows compared with

dilute flows inferred for the deposition of Facies 4. Consequently, these flows may have been initiated closer to the source of terrestrial organic debris i.e. the fluvio-deltaic plains fringing the London-Wales-Brabant High, and had a wider distribution. They are likely linked to phases of increased fluvial run-off or storm-generated currents (cf. Davies et al., 2012). Due to similar settling velocities of sporomorphs and fine silt (Stanley, 1965), sporomorphs (and sporomorph-sized phytoclasts) tend to be associated primarily with the graded silt-bearing beds of Facies 5. This also demonstrates the importance of water transport through offshore-directed underflows for sporomorph dispersion (cf. Muller, 1959). In contrast, Facies 6 shows a greater grain size distribution; this might explain the high proportions of gelified OM which also has a wide size range. However, some samples (sample 1, sample 55), show that this pattern may not apply for individual turbidite beds and, in fact, it is not clear whether sedimentary or preservational processes control the ratio of land plant material-derivatives, i.e. between gelified OM and phytoclasts. The AOM_{Gr} and AOM_{Br} fractions contained in these facies likely result from turbulent mixing of unconsolidated clay-rich sediment and entrainment of overlying water with the flows (cf. Mulder and Alexander, 2001). Facies 7 is interpreted as the deposits of non-turbulent sediment gravity flows (debris flows) dominated by land plant material (G and subordinate Ph_{Br}), but low in AOM_{Gr} . The unusually high HI displayed by the other sample of this facies (Sample 21) is perhaps explained by high content of higher plant derivatives, for example cuticular material (cf. Talbot and Livingstone, 1989).

The abundance of AOM_{Gr} and AOM_{Br} in the lower Carsington section (below 33.85 m) suggest that phytoplanktonic algae and bacteria delivered to the sediment surface via hemipelagic settling. The land plant-derived material, in the form of gelified particles, phytoclasts and sporomorphs are associated with facies interpreted as sediment density flows (turbidity and debris flows) which were likely sourced from near-shore deltaic environments. These findings support earlier studies (e.g. Jäger, 2004; Davies et al., 2012), documenting that different sediment delivery processes, and

not necessarily a change in palaeoenvironmental conditions may account for variations in OM composition.

The dominance of algal-derived AOM_{Gr} with some AOM_{Br} suggests that the water column is the predominant source of material, as in clay-rich mudstones (Facies 4) below 33.85 m. This is consistent with microtextural information from lenticular clay-rich layers, indicating hemipelagic settling of flocculated organo-mineralic aggregates, faecal pellets and goniatite shells with limited advective transport. Interbedded silt-bearing layers were likely deposited from the downward supply of silt- and clay-grade material from buoyant detached turbid suspensions. Buoyant freshwater plumes, which may have acted as the main transport mechanism for terrestrially-derived OM, were likely transported from river mouths into the basin, traveling above density interfaces (cf. Nemeč, 1995). Similar plumes of suspended material may be initiated by storms. The plant fragments delivered by these plumes provided substrates for the formation of AOM_{Br} during their descent through the water column, which can explain the increased abundance of AOM_{Br} in some samples. Continuous hemipelagic settling of flocculated material (AOM_{Gr}) was the dominant depositional process, accompanied by the intermittent supply (except in a few samples) of silt-grade terrestrially-derived material from suspension plumes.

Noticeable proportions of algae remains and cysts are only present in one calcareous mudstone sample (103, Facies 2) that was deposited during intervals of very high phytoplankton productivity in the water column (Könitzer et al., 2014). Zooplankton (radiolaria), which were described by Holdsworth (1966) presumably drew on the phytoplankton resulting in significant accumulations of planktonic OM with minimal clastic dilution. Although most of the organic material delivered to the sediment-water interface was degraded and mineralised by microbial activity, some remains of algae are preserved.

The total abundance and the diversity of sporomorphs decrease into the top part of the section. Such trends are characteristic of transitions from relatively proximal to more distal settings (Jäger, 2004). The more dramatic decline in forest-mire and non-forest mire groups compared with

colonisers and monosaccate pollen (cordaitaleans) may suggest a stronger disturbance of the wetland communities in response to rising sea-level (Turner et al., 1994), whereas plants belonging to the colonisers and cordaites may have been adapted to a wider range of habitats and were less affected.

The sedimentological characteristics and OM composition of mudstones above 33.85 m are consistent with the presence of marine macrofauna (*E. yatesae* and *Ct. edalensis*), indicating deposition in a fully marine basin. The depositional setting did not change from the lowstand deposition (below 33.85 m) but the marine transgression, indicated by the presence of the goniatites (Waters and Condon, 2012), resulted in an increased distance to the shoreline placing this location out of reach of sediment density flows. OM deposition was, therefore, less affected by clastic dilution despite some siliciclastic supply from detached turbid flows. If the sedimentation rates were low however, longer exposure at the sediment-water interface, compared with rapid burial of OM by sediment density flows, would have oxidised the organic matter. Thus, lower clastic dilution is unlikely to be the main factor for the increased TOC of this unit. Instead a balance of lower siliciclastic dilution and enhanced phytoplankton productivity during sea-level transgressions likely accounts for higher OM burial rates (see Könitzer et al., 2014).

Phytoplankton productivity fuelled carbonate productivity in the photic zone and resulted in a greater OM flux (mainly AOM_{Gr}) to the sea-floor.

5.3. *Palaeoenvironmental changes interpreted from sporomorph data*

The sporomorph assemblages (Figs. 7, 8) below 33.85 m indicate a predominance of the ‘wetland’ flora (Turner and Spinner, 1993; Turner et al., 1994), represented by the forest mire and non-forest mire ecological groups. The assemblages displayed in the bottom part of the section are typical for sea-level lowstands, when large low-lying deltaic plains were densely vegetated (e.g. Turner and Spinner, 1993; Davies and McLean, 1996; Stephenson et al., 2008). This is also supported by high diversity of sporomorph genera (Fig. 8).

The sporomorph assemblages above 33.85 m are similar to typical trends for Namurian mudstone strata containing marine bands (e.g. Turner et al., 1994; Davies and McLean, 1996; Hawkins et al., 2013). The total abundance and the diversity of sporomorphs decrease into the top part of the section. Such trends are characteristic of transitions from relatively proximal to more distal settings (Turner et al., 1994; Jäger, 2004). The sea-level rise increased the distance to the palaeo-shoreline, resulting in relatively fewer sporomorphs reaching the area of deposition. Nevertheless, the changes in relative abundances of sporomorph groups suggest that plant communities themselves were also affected by the sea-level rise. The more dramatic upward decline in forest-mire and non-forest mire groups (Turner et al., 1994) may suggest a stronger disturbance of the parent wetland communities, which are thought to inhabit solely coastal swamps and floodplains, during rising sea level (Turner and Spinner, 1993). Sporomorphs of colonisers and monosaccate pollen also decrease upward but their relative proportions are highest in the top section in some assemblages from Facies 1 and 3 (most notably the major occurrence of monosaccate pollen at 15.50 m). The parent plant groups, Sigillariaceae and Cordaites respectively, were presumably adapted to a wider range of habitats and were less affected by a retrograding shoreline (Neves, 1958), although Stephenson et al. (2008) questioned whether these plant groups had developed a drier substrate affinity before the end of the Arnsbergian. This also appears to be the case in the deltas fringing the southern margin of the Widmerpool Gulf, despite the fact that the deltas at the southern margin of the Widmerpool Gulf were of small extent and did not prograde far into the basin (Holdsworth and Collinson, 1988).

Within the 'wetland' community, the contribution of the forest mire group to the assemblages declines upwards more strongly, whereas the non-forest mire (derived from ferns and pteridosperms) forms the major group in the top of the section. The reasons behind this tendency are not clear as the known ecological habitat of fern-like plants on floodplains would not be expected to decline stronger than swamp areas, which were dominated by lycosids (Scott, 1979).

5.4. Gas source rock potential

Combined optical palynofacies and Rock-Eval data (Figs. 10, 11a) show an approximate relationship between the abundance of AOM_{Gr} and hydrogen index (with the exception of Facies 7). Samples rich in AOM_{Gr} (Facies 1, 2, 3, 4a and some samples of Facies 4b) tend to be associated with type II kerogen, and as such are oil- and gas-prone (Tissot and Welte, 1984; Dahl et al., 2004). In turn, samples showing significant proportions of land-derived OM (Facies 4c, 5, 6 and few samples of Facies 4b) contain mixtures of type II and type III kerogen, or predominantly type III, and are therefore more gas-prone. This indicates that AOM_{Gr} is the most prolific OM constituent with regard to hydrocarbon generation potential.

In addition, the AOM_{Gr}-rich facies tend to have higher TOC (above 2%, derived from Rock-Eval) and therefore show high S₂ values, indicative that significant volumes of hydrocarbons could be generated by these mudstones. Consequently, Facies 1 mudstones would be most prospective as source rocks, followed by Facies 3 and 4a. Facies 4b, 4c, 5 and 6 could source some hydrocarbons but have a lower hydrocarbon potential. Facies 2 is not considered for reasons discussed in section 3.3.

To be regarded as a potential target for thermogenic shale gas, organic-rich mudstones with this OM composition (predominantly type II) would need to have reached thermal maturity equivalent to the dry gas window (vitrinite reflectance $R_0 > 1.35\%$). In this case, as the OM progresses from the oil window (vitrinite reflectance $R_0 = 0.5-1.3\%$), where both liquid and gaseous hydrocarbons would be present, to the dry gas window, gas compounds would be directly expelled from the kerogen, but also from secondary cracking of oil compounds (e.g. Hill et al., 2007), leading to a gas phase-dominated hydrocarbon composition.

6. CONCLUSIONS

The early Namurian (late Mississippian, Arnsbergian) organic-rich mudstones encountered at Carsington, Derbyshire were deposited in a confined deep-marine setting in the Widmerpool Gulf. The location was within the reach of distal sediment gravity flows from vegetated deltas during sea-level lowstands, whereas during marine transgressions shorelines migrated landward and hemipelagic suspension settling, under high planktonic productivity, was dominant.

The organic matter (OM) examined on palynological slides can be related to two main sources:

- I) The autochthonous marine OM includes a main granular translucent amorphous type (AOM_{Gr}), likely composed of degraded phytoplanktonic algae and microbes, and few preserved algal remains.
- II) Allochthonous terrestrial OM is represented by gelified OM fragments, derived from chemically altered land plant material, black opaque and brown phytoclasts, and subordinate sporomorphs. A brown amorphous type (AOM_{Br}) of OM, likely derived from the assimilation of land plant fragments by microbial communities, contains both autochthonous and allochthonous constituents.

AOM_{Gr} is the major constituent in all clay-rich lithofacies and corresponds to kerogen type II, with a very minor terrestrial OM contribution. Interbedded sand-bearing and silt-rich mudstones present in the basal section have moderate AOM_{Gr} proportions and more significant contributions from terrestrial OM, thus these facies typically have mixtures of type II and III kerogens.

The visually determined OM composition is in good agreement with geochemical parameters: the ratio of AOM_{Gr} and plant material is positively correlated with bulk $\delta^{13}\text{C}_{\text{org}}$ and hydrogen index (HI). This suggests that AOM_{Gr} constitutes the main oil and gas expelling component in this section. The AOM_{Gr}-rich mudstones, that include the *E. yatesae* and *Ct. edalensis* marine bands, represent the most prospective intervals for the generation of thermogenic shale gas and were deposited during phases of high phytoplankton and carbonate productivity as sea-levels rose. The thin-bedded clay-rich mudstones and sand-bearing and silt-rich beds deposited during lower sea-

level should not be disregarded as potential shale gas targets given the abundance of AOM_{Gr} , in addition to the terrestrial OM.

Our results indicate that, for the basinal environment of the Widmerpool Gulf, sea-level fluctuations influence the bioproductivity and therefore absolute OM content, whereas the OM composition, the balance between AOM_{Gr} and terrestrial OM, was influenced more strongly by sediment delivery processes. These findings highlight the gas source rock potential of basinal mudstone successions, particularly those deposited during transgressive and highstand periods and, for the first time in the Carboniferous, provides the evidence for the explicit link between the abundance of translucent amorphous matter (AOM_{Gr}) from degraded phytoplanktonic algae and microbes and the dominance of type II kerogens. Linking palynofacies typing, sporomorph counts and Rock-Eval data to the carbon-isotope values of the bulk organic matter ($\delta^{13}\text{C}_{\text{org}}$) demonstrates that the $\delta^{13}\text{C}_{\text{org}}$ provides a relatively rapid and informative assessment of the likely kerogen type. The multidisciplinary approach applied here provides insight into the main sedimentological and palaeoenvironmental controls underpinning the shale gas generation potential of fine-grained sedimentary rocks.

ACKNOWLEDGEMENTS

The authors would like to thank Jane Flint for palynological preparations and Christopher Kendrick for performing $\delta^{13}\text{C}$ analyses. Anthony Milodovski is thanked for support with UV fluorescence microscopy. Mike Purnell and Stewart Molyneux are gratefully acknowledged for discussions. We would also like to thank the editor, Hans Kerp, for handling the manuscript and two reviewers for their helpful comments. Financial support to Könitzer for this PhD project from the University of Leicester and from the British Geological Survey University Funding Initiative (BUFI) is gratefully acknowledged. Mike Stephenson and Christopher Vane publish with the permission of the Director of the British Geological Survey.

REFERENCES

- Aitkenhead, N., 1977. The Institute of Geological Sciences Borehole at Duffield, Derbyshire. Her Majesty's Stationery Office, London.
- Aitkenhead, N., 1991. Carsington Dam Reconstruction - Notes on the stratigraphy and correlation of groundwater monitoring boreholes. Unpublished report prepared for Babbie Shaw & Morton, British Geological Survey W2/90/5.
- Aitkenhead, N., Barclay, W.J., Brandon, A., Chadwick, R.A., Chisholm, J.I., Cooper, A.H., Johnston, E.W., 2002. British Regional Geology: The Pennines and Adjacent Areas. Her Majesty's Stationery Office, London.
- Ando, A., Kakegawa, T., Takashima, R., Saito, T., 2003. Stratigraphic carbon isotope fluctuations of detrital woody materials during the Aptian Stage in Hokkaido, Japan: Comprehensive $\delta^{13}\text{C}$ data from four sections of the Ashibetsu area. *J. Asian Earth Sci.* 21, 835-847.
- Aplin, A.C., Macquaker, J.H.S., 2011. Mudstone diversity: Origin and implications for source, seal, and reservoir properties in petroleum systems. *AAPG Bull.* 95, 2031-2059.
- Batten, D.J., 1983. Identification of Amorphous Sedimentary Organic Matter by Transmitted Light Microscopy. In: Brooks, J. (Ed.), *Petroleum Geochemistry and Exploration of Europe*. Academic Press, London, pp. 275-287.
- Batten, D.J., 1996. Palynofacies and palaeoenvironmental interpretation, in Jansonius, J., McGregor, D.C. (Eds.), *Palynology: Principles and Applications*. American Association of Stratigraphic Palynologists Foundation, pp. 1011-1064.
- Boussafir, M., Gelin, F., Lallier-Vergès, E., Derenne, S., Bertrand, P., Largeau, C., 1995. Electron microscopy and pyrolysis of kerogens from the Kimmeridge Clay Formation, UK: Source organisms, preservation processes, and origin of microcycles. *Geochim. Cosmochim. Acta* 59, 3731-3747.
- Brandon, A., Riley, N.J., Wilson, A.A., Ellison, R.A., 1995. Three new early Namurian (E_{1c} - E_{2a}) marine bands in central and northern England, UK, and their bearing on correlations with the Askrigg Block. *Proc. Yorks. Geol. Soc.* 50, 333-355.
- Chisholm, J.I., Charsley, T.J., Aitkenhead, N., 1988. Geology of the Country around Ashbourne and Cheadle. Memoir of the British Geological Survey 124. Her Majesty's Stationery Office, London.
- Collinson, J.D., 1988. Controls on Namurian sedimentation in the Central Province basins of northern England. In: Besly, B.M., Kelling, G. (Eds.), *Sedimentation in a Synorogenic Basin Complex: The Upper Carboniferous of Northwest Europe*. Blackie, Glasgow and London, pp. 85-101.
- Combaz, A., 1980. Les kérogènes vus au microscope. In: Durand, B. (Ed.), *Kerogen - Insoluble Organic Matter from Sedimentary Rocks*. Éditions Technip, Paris, pp. 55-112.

Dahl, B., Bojesen-Koefoed, J., Holm, A., Justwan, H., Rasmussen, E., Thomsen, E., 2004. A new approach to interpreting Rock-Eval S2 and TOC data for kerogen quality assessment. *Org. Geochem.* 35, 1461-1477.

Davies, S.J., 2008. The record of Carboniferous sea-level change in low-latitude sedimentary successions from Britain and Ireland during the onset of the late Paleozoic ice age. In: Fielding, C.R., Frank, T.D., Isbell, J.L. (Eds.), *Resolving the Late Paleozoic Ice Age in Time and Space*, Geological Society of America Special Paper 441, pp. 187-204.

Davies, S.J., McLean, D., 1996. Spectral gamma-ray and palynological characterization of Kinderscoutian marine bands in the Namurian of the Pennine Basin. *Proc. Yorks. Geol. Soc.* 51, 103-114.

Davies, S.J., Leng, M.J., Macquaker, J.H.S., Hawkins, K., 2012. Sedimentary process control on carbon isotope composition of sedimentary organic matter in an ancient shallow-water shelf succession. *Geochem. Geophys. Geosys.* 13, Q0AI04.

Department of Energy & Climate Change (DECC), 2010. *The Unconventional Resources of Britain's Onshore Basins - Shale Gas*, DECC, London.

Disnar, J.R., Guillet, B., Keravis, D., Di-Giovanni, C., Sebag, D., 2003. Soil organic matter (SOM) characterization by Rock-Eval pyrolysis: scope and limitations. *Org. Geochem.* 34, 327-343.

Eisma, D., 1986. Flocculation and de-flocculation of suspended matter in estuaries. *Neth. J. Sea Res.* 20, 183-199.

Ercegovac, M., Kostić, A., 2006. Organic facies and palynofacies: Nomenclature, classification and applicability for petroleum source rock evaluation. *Int. J. Coal Geol.* 68, 70-78.

Falcon-Lang, H.J., 2004. Pennsylvanian tropical rain forests responded to glacial-interglacial rhythms. *Geology* 32, 689-692.

Falcon-Lang, H.J., Benton, M.J., Braddy, S.J., Davies, S.J., 2006. The Pennsylvanian tropical biome reconstructed from the Joggins Formation of Nova Scotia, Canada. *J. Geol. Soc.* 163, 561-576.

Fielding, C.R., Frank, T.D., Isbell, J.L., 2008. The late Paleozoic ice age: A review of current understanding and synthesis of global climate patterns. In: Fielding, C.R., Frank, T.D., Isbell, J.L., (Eds.), *Resolving the Late Paleozoic Ice Age in Time and Space*. Geological Society of America Special Paper 441, pp. 343-354.

Frank, M.C., Tyson, R.V., 1995. Parasequence-scale organic facies variations through an Early Carboniferous Yoredale cyclothem, Middle Limestone Group, Scremerston, Northumberland. *J. Geol. Soc.* 152, 41-50.

Fraser, A.J., Gawthorpe, R.L., 2003. *An Atlas of Carboniferous Basin Evolution in Northern England*. Geological Society of London Memoir 28, The Geological Society, London.

- Fraser, A.J., Nash, D.F., Steele, R.P., Ebdon, C.C., 1990. A regional assessment of the intra-Carboniferous play of Northern England. In: Brooks, J. (Ed.), *Classic Petroleum Provinces*. The Geological Society, London, pp. 417-440.
- Gregory, W.A., Chinn, E.W., Sassen, R., Hart, G.F., 1991. Fluorescent microscopy of particulate organic matter: Sparta Formation and Wilcox Group, South Central Louisiana. *Org. Geochem.* 17, 1-9.
- Hampson, G.J., Elliott, T., Davies, S.J., 1997. The application of sequence stratigraphy to Upper Carboniferous fluvio-deltaic strata of the onshore UK and Ireland: implications for the southern North Sea. *J. Geol. Soc.* 154, 719-733.
- Hart, G.F., 1986. Origin and classification of organic matter in clastic systems. *Palynology* 10, 1-23.
- Hawkins, K., Davies, S.J., Mullins, G.L. and Macquaker, J.H.S., 2013. Miospore distribution and sedimentological facies distribution as an insight to changing terrestrial palaeoequatorial floral communities during a Pennsylvanian glacio-eustatic sea level cycle. *Rev. of Palaeobot. Palynol.* 197, 166-178.
- Highton, P.J.C., Pearson, A., Scott, A.C., 1991. Palynofacies and palynodebris and their use in Coal Measure palaeoecology and palaeoenvironmental analysis. *N. Jb. Geol. Paläont. Abh.* 183, 135-169.
- Hill, R.J., Jarvie, D.M., Zumberge, J., Henry, M., Pollastro, R.M., 2007. Oil and gas geochemistry and petroleum systems of the Fort Worth Basin. *AAPG Bull.* 91, 445-473.
- Holdsworth, B.K., 1966. A preliminary study of the palaeontology and palaeoenvironment of some Namurian limestone 'bullions'. *J. East Mids. Geol. Soc.* 1, 315-338.
- Holdsworth, B.K., Collinson, J.D., 1988. Millstone Grit cyclicity revisited. In: Besly, B.M., Kelling, G. (Eds.), *Sedimentation in a Synorogenic Basin Complex: The Upper Carboniferous of Northwest Europe*. Blackie, Glasgow and London, pp. 132-152.
- Jäger, H., 2004. Facies dependence of spore assemblages and new data on sedimentary influence on spore taphonomy. *Rev. Palaeobot. Palynol.* 130, 121-140.
- Jones, R.W., 1987. Organic Facies. In: Brooks, J., Welte, D.H. (Eds.), *Advances in Petroleum Geochemistry Vol. 2*. Academic Press, London, pp. 1-90.
- Kombrink, H., 2008. *The Carboniferous of the Netherlands and Surrounding Areas; a Basin Analysis*: PhD Thesis, Utrecht University.
- Könitzer, S.F., Leng, M.J., Davies, S.J., Stephenson, M.H., 2012. An assessment of geochemical preparation methods prior to organic carbon concentration and carbon isotope ratio analyses of fine-grained sedimentary rocks. *Geochem. Geophys. Geosys.* 13, Q0AI02.
- Könitzer, S.F., Davies, S.J., Stephenson, M.H., Leng, M.J., 2014. Depositional controls on mudstone lithofacies in a basinal setting – implications for the delivery of sedimentary organic matter. *J. Sed. Res.* 84, 198-214.

- Lewan, M.D., 1986. Stable carbon isotopes of amorphous kerogens from Phanerozoic sedimentary rocks. *Geochim. Cosmochim. Acta* 50, 1583-1591.
- Mann, U., Hantschel, T., Schaefer, R.G., Krooss, B., Leythaeuser, D., Littke, R., Sachsenhofer, R.F., 1997. Petroleum Migration: Mechanisms, Pathways, Efficiencies, and Numerical Simulations. In: Welte, D.H., Horsfield, B., Baker, D.R. (Eds.), *Petroleum and Basin Evolution*. Springer-Verlag, Berlin, pp. 403-520.
- Masran, T.C., Pocock, S.A.J., 1981. The Classification of Plant-derived Particulate Organic Matter in Sedimentary Rocks. In: Brooks, J. (Ed.), *Organic Maturation Studies and Fossil Fuel Exploration*. Academic Press, London, pp. 145-176.
- Maynard, J.B., 1981. Carbon isotopes as indicators of dispersal patterns in Devonian-Mississippian shales of the Appalachian Basin. *Geology* 9, 262-265.
- Mulder, T., Alexander, J., 2001. The physical character of subaqueous sedimentary density flows and their deposits. *Sedimentology* 48, 269-299.
- Muller, J., 1959. Palynology of Recent Orinoco Delta and shelf sediment: reports of the Orinoco Shelf expedition, volume 5. *Micropaleontology* 5, 1-32.
- Nemec, W., 1995. The dynamics of deltaic suspension plumes. In: Oti, M.N., Postma, G. (Eds.), *The Geology of Deltas*. A. A. Balkema, Rotterdam, pp. 31-93.
- Neves, R., 1958. Upper Carboniferous plant spore assemblages from the *Gastrioceras subcrenatum* horizon, north Staffordshire. *Geol. Mag.* 95, 1-19.
- Pacton, M., Gorin, G.E., Vasconcelos, C., 2011. Amorphous organic matter — Experimental data on formation and the role of microbes. *Rev. Palaeobot. Palynol.* 166, 253-267.
- Passey, Q.R., Bohacs, K.M., Esch, W.L., Klimentidis, R., Sinha, S., 2010. From Oil-Prone Source Rock to Gas-Producing Shale Reservoir - Geologic and Petrophysical Characterization of Unconventional Shale-Gas Reservoirs. *SPE 131350*, 29.
- Peters-Kottig, W., Strauss, H., Kerp, H., 2006. The land plant $\delta^{13}\text{C}$ record and plant evolution in the Late Palaeozoic. *Palaeogeogr., Palaeoclimatol., Palaeoecol.* 240, 237-252.
- Powell, T.G., Creaney, S., Snowdon, L.R., 1982. Limitations of use of organic petrographic techniques for identification of petroleum source rocks. *AAPG Bull.* 66, 430-435.
- Ramsbottom, W.H.C., 1977. Major Cycles of Transgression and Regression (Mesothems) in the Namurian. *Proc. Yorks. Geol. Soc.* 41, 261-291.
- Riegel, W., 2008. The Late Palaeozoic phytoplankton blackout — Artefact or evidence of global change? *Rev. Palaeobot. Palynol.* 148, 73-90.
- Roche, I.P., 2012. Lessons from History - Unlocking a New UK Shale Oil Play. *SPE 150933* .
- Schiøler, P., Rogers, K., Sykes, R., Hollis, C.J., Ilg, B., Meadows, D., Roncaglia, L., Uruski, C., 2010. Palynofacies, organic geochemistry and depositional environment of the Tartan Formation

- (Late Paleocene), a potential source rock in the Great South Basin, New Zealand. *Mar. Pet. Geol.* 27, 351-369.
- Scott, A.C., 1979. The ecology of Coal Measure floras from northern Britain. *Proc. Geol. Assoc.* 90, 97-116.
- Sebag, D., Copard, Y., Di-Giovanni, C., Durand, A., Laignel, B., Ogier, S., Lallier-Verges, E., 2006. Palynofacies as useful tool to study origins and transfers of particulate organic matter in recent terrestrial environments: Synopsis and prospects. *Earth-Sci. Rev.* 79, 241-259.
- Selley, R.C., 2012. UK shale gas: The story so far. *Mar. Pet. Geol.* 31, 100-109.
- Smith, N., Turner, P., Williams, G., 2010. UK data and analysis for shale gas prospectivity. *Geol. Soc. Petroleum Geology Conference Series* 7, 1087-1098.
- Spears, D.A., Amin, M.A., 1981. Geochemistry and mineralogy of marine and non-marine Namurian black shales from the Tansley Borehole, Derbyshire. *Sedimentology* 28, 407-417.
- Stanley, E.A., 1965. Abundance of pollen and spores in marine sediments. *Southeastern Geologist* 7, 25-33.
- Stephenson, M.H., Williams, M., Leng, M., Monghan, A.A., 2004. Aquatic plant microfossils of probable non-vascular origin from the Ballagan Formation (Lower Carboniferous), Midland Valley, Scotland. *Proc. Yorks. Geol. Soc.* 55, 145-158.
- Stephenson, M.H., Leng, M.J., Vane, C.H., Osterloff, P.L., Arrowsmith, C., 2005. Investigating the record of Permian climate change from argillaceous sedimentary rocks, Oman. *J. Geol. Soc.* 162, 641-651.
- Stephenson, M.H., Millward, D., Leng, M.J., Vane, C.H., 2008. Palaeoecological and possible evolutionary effects of early Namurian (Serpukhovian, Carboniferous) glacioeustatic cyclicity. *J. Geol. Soc.* 165, 993-1005.
- Stephenson, M.H., Angiolini, L., Cozar, P., Jadoul, F., Leng, M.J., Millward, D., Chenery, S., 2010. Northern England Serpukhovian (early Namurian) farfield responses to southern hemisphere glaciation. *J. Geol. Soc.* 167, 1171-1184.
- Talbot, M.R., Livingstone, D.A., 1989. Hydrogen index and carbon isotopes of lacustrine organic matter as lake level indicators. *Palaeogeogr., Palaeoclimatol., Palaeoecol.* 70, 121-137.
- Tissot, B.P., Welte, D.H., 1984. *Petroleum Formation and Occurrence*, 2 ed. Springer Verlag, Berlin.
- Traverse, A., 1988. *Paleopalynology*. Unwin Hyman, Boston.
- Trewin, N.H., Holdsworth, B.K., 1973. Sedimentation in the Lower Namurian Rocks of the North Staffordshire Basin. *Proc. Yorks. Geol. Soc.* 39, 371-408.
- Turner, N., Spinner, E., 1993. A palynostratigraphic study of Namurian-Westphalian deltaic sequences of the southern Central Pennine Basin, Derbyshire, England. *Rev. Palaeobot. Palynol.* 77, 23-43.

- Turner, N., Spinner, E., Spode, F., Wignall, P.B., 1994. Palynostratigraphy of a transgressive systems tract from the earliest Alportian (Namurian) of Britain. *Rev. Palaeobot. Palynol.* 80, 39-54.
- Tyson, R.V., 1987. The genesis and palynofacies characteristics of marine petroleum source rocks. In: Brooks, J., Fleet, A.J. (Eds.), *Marine Petroleum Source Rocks*. Geol. Soc. Spec. Publ. 26, pp. 47-67.
- Tyson, R.V., 1995. *Sedimentary Organic Matter*. Chapman and Hall, London.
- Venkatachala, B.S., 1981. Differentiation of Amorphous Organic Matter Types in Sediments. In: Brooks, J. (Ed.), *Organic Maturation Studies and Fossil Fuel Exploration*. Academic Press, London, pp. 177-200.
- Waters, C.N., Davies, S.J., 2006. Carboniferous: extensional basins, advancing deltas and coal swamps. In: Brenchley, P.J., Rawson, P.F. (Eds.), *The Geology of England and Wales*. The Geological Society, London, pp. 173-224.
- Waters, C.N., Condon, D.J., 2012. Nature and timing of Late Mississippian to Mid-Pennsylvanian glacio-eustatic sea-level changes of the Pennine Basin, UK. *J. Geol. Soc.* 167, 37-51.
- Wenger, L.M., Baker, D.R., Chung, H.M., McCulloh, T.H., 1988. Environmental control of carbon isotope variations in Pennsylvania black-shale sequences, Midcontinent, U.S.A. *Org. Geochem.* 13, 765-771.
- Whitaker, M.F., Giles, M.R., Cannon, S.J.C., 1992. Palynological review of the Brent Group, UK sector, North Sea. In: Morton, A.C., Haszeldine, R.S., Giles, M.R., Brown, S. (Eds.), *Geology of the Brent Group*. Geol. Soc. Spec. Publ. 61, pp. 169-202.
- Wood, G.D., Gabriel, A.M., Lawson, J.C., 1996. Palynological techniques - processing and microscopy. In: Jansonius, J., McGregor, D.C. (Eds.), *Palynology: Principles and Applications*. American Association of Stratigraphic Palynologists Foundation, pp. 29-50.
- Wood, G.D., Palmer-Koleman, S.E., Alemán, A.M., Padilla, H., 2002. Palynofacies and biomarker analysis of the lowermost Permo-Carboniferous Pular Formation, a volcanic arc sequence in the Sierra de Almeida, Northern Chile. *Rev. Palaeobot. Palynol.* 118, 323-333.

FIGURE CAPTIONS

Figure 1: Location of the study area and geological context of the Carsington Dam Reconstruction C4 borehole. a) Geological map of the study area – after Aitkenhead et al. (2002). b) Early Arnsbergian palaeogeography of Britain – redrawn after Fraser and Gawthorpe (2003); Waters and Davies (2006); Davies et al. (2012a). Study area highlighted. c) Detailed sedimentary log of

the Carsington core material, with observations from the report by Aitkenhead (1991). Samples used for palynological preparation are highlighted.

Figure 2: Overview of lithofacies characteristics and basin model of early Namurian mudstones at Carsington (after Köntzer et al., 2014).

Figure 3: Profile of the Carsington Dam C4 core material showing the palynofacies composition (in % of total organic matter). Gelified OM (G) and algal remains (A) are displayed in counts (out of 500).

Figure 4: Bar chart showing the mean palynofacies composition of each lithofacies. Note that the compositions of Facies 2, 4c and 7 are based on one sample each.

Figure 5: Profile of the Carsington Dam C4 core material showing the visually determined amount of sporomorphs (S; highlighted) and calculated amounts of the other palynofacies groups as per g measurements. For lithofacies key see Figure 3.

Figure 6: Plot of TOC (derived from EA data) against the total amount of organic residue of the sample processed for quantitative palynology (calculated as the sum of all palynofacies groups).

Figure 7: Profile of the Carsington Dam C4 core material showing the abundance of sporomorphs according to their parent ecological groups. Numbers refer to the numbers of sporomorph recorded per slide. For lithofacies key see Figure 3.

Figure 8: Profile of the Carsington Dam C4 core material showing the abundance of sporomorphs according to their parent ecological groups as a percentage of the sum of all ecological groups. For lithofacies key see Figure 3.

Figure 9: Crossplot showing bulk $\delta^{13}\text{C}_{\text{org}}$ against the point-counted relative proportions of AOM_{Gr} and G plus Ph_{total} , respectively, per sample.

Figure 10: Modified van Krevelen diagram combining Rock-Eval parameters and lithofacies information.

Figure 11: a) Crossplot showing the proportion of AOM_{Gr} and hydrogen indices from Rock-Eval Pyrolysis. b) S2-TOC plot of all Rock-Eval samples. TOC data is derived from Rock-Eval Pyrolysis. For lithofacies key see Figure 3.

Plate I: Photomicrographs taken under transmitted white light illustrating the appearance of AOM_{Gr} and AOM_{Br} : 1 – sample 103) translucent AOM_{Gr} with few inclusions; 2– sample 83) AOM_{Br} particle with prominent massive inner zone bordered by more translucent granular material (margin indicated by dashed line). Around some of the particle's angular corners sharp outlines of the inner zone are visible (arrow); 3 – sample 103) AOM_{Gr} with abundant inclusions and characteristically diffuse edges (arrows); 4 – sample 83) fragment with granular amorphous texture, but obvious structured aspect. The particle shows a cross-hatched structure (arrow), as characteristic of xylem tissues of land plants; 5 – sample 64) slightly dark AOM_{Gr} particle with larger opaque inclusions (arrows); 6 – sample 42) massive particle with an overall elongated shape, reminiscent of phytoclasts. One edge is planar and relatively sharp (arrow) while the long ends have a fringe of diffuse, granular amorphous material (dashed arrow); 7 –sample 35) particle with fine granular texture, created by μm -scale opaque phytoclasts fragments and pyrite; 8 – sample 24) large, massive, fluffy particle showing oval holes that are filled by translucent, granular material (arrow). Granular material is also surrounding the particle in places (dashed arrows); 9 – sample 100) AOM_{Gr} particle with no obvious structure. Small holes (solid red arrows), probably due to dissolution of mineral grains, and micrometre-size inclusions (dashed yellow arrows) are visible; 10 – sample 29) AOM_{Br} particle showing a partly structured aspect, with one clear edge (solid red arrow) and two faint parallel ridge (dashed yellow arrows). Surface of the particle is amorphous. The magnified image reveals presence of typical xylem tissue structure.

Plate II: Photomicrographs of selected palynofacies groups: 1 – sample 49) gelified OM particle, which exhibits a similar shape as phytoclasts and slightly irregular outlines, but lacks internal

structure and is therefore massive; 2 – sample 43) vitrinite particle (arrow), internally homogenous with slight lustre, with very sharp edges (typical of sub-conchoidal fracture). Vitrinites are counted as part of gelified OM. This image also shows smaller black opaque phytoclasts (dashed arrows); 3 – sample 49) elongated black phytoclast characterised by smooth, sharp edges and black opaque colour. The regular arrangement of small circular pits (arrow) indicate relict biostructure, probably of land plant origin; 4 – sample 26) well-preserved brown phytoclast. The elongated cellular structure suggests part of a leaf cuticle; 5 – sample 103) translucent-yellow thin sheet (arrow), perhaps of marine algal origin. Outlines are slightly better defined than for AOM_{Gr} particles; 6 – sample 56) ‘tube-like’ particle composed of very thin translucent-yellow material (arrow), possibly of marine algal origin.

Plate III: Photomicrographs of palynological slides under transmitted white light (left side) and under UV light excitation (right). 1) Sample 103 (from a concretionary calcareous mudstone) showing discrete (<100 µm) translucent granular AOM_{Gr} particles with relatively few inclusions. The orange to yellow fluorescence indicate a possible algal source material. Small image (A’) taken at double magnification shows algal test characterised by very high fluorescence. 2) Sample 95 (from a lenticular clay-dominated mudstone) is dominated by AOM_{Gr}, and some particles with an inner gelified aspect (AOM_{Br}); however all amorphous particles show the same patchy fluorescence properties. Black phytoclast (Ph_{Bl}) can be distinguished by lack of fluorescence. 3) Sample 81 (from a lenticular clay-dominated mudstone) depicting dominant >100 µm, often coherent AOM_{Gr}. All of these particles, regardless of translucence and abundance of inclusions are characterised by a patchy moderate to high fluorescence. Faint spore grain (S) is visible due to high yellow-orange fluorescence; in contrast Ph_{Bl} is non-fluorescent. 4) Sample 63 (from a sand-bearing silt-rich mudstone) depicting a mixed palynofacies assemblage including structured brown phytoclasts (Ph_{Br}) and gelified OM (G), both showing weak fluorescence around the particle margins, and non-fluorescent lath-shaped Ph_{Bl} fragments. Discrete grains of AOM_{Gr} have a dull or stronger yellow fluorescence. Spores display the highest fluorescence intensity.

All scale bars are 100 μm long. Note that dark green background is imposed by Elvacite.

Plate IV: Photomicrographs of sporomorph genera, with England Finder reference number: a)

Lycospora spp. sample 43, slide (2)4, D23/3; b) *Densosporites* spp. sample 57, slide (1)2, L27/4;

c) *Granulatisporites* spp. sample 57, slide (1)2, C30/-; d) *Leiotriletes* spp. sample 13, slide (2)6,

U13/-; e) *Punctatisporites* spp. sample 43, slide (2)4, N47/4; f) *Verrucosisorites* spp. sample 67,

slide (1)3, J21/3; g) *Crassispora* spp. Sample 79, slide (3)8, V34/-; h) *Florinites* spp. Sample 13,

slide (2)6, X23/-. All scale bars are 50 μm .

TABLES

Category	Group	Description
Amorphous organic matter (AOM)	AOM _{Gr} Granular translucent AOM	Heterogeneous, colourless to dark grey particles with diffuse edges and inclusions of other particles Moderate to strong patchy fluorescence
	AOM _{Br} Brown AOM	Similar to granular translucent AOM, but with inner gelified aspect Moderate patchy fluorescence
Gelified organic matter	G Gelified OM (including vitrinite)	Black, dark brown or amber lustrous particles, lacking internal structure. Dull irregular or smooth edges Weakly fluorescent
Phytoclasts (Ph _{total})	Ph _{Bl} Black opaque phytoclasts	Opaque angular clasts or laths Non-fluorescent
	Brown phytoclasts	Brown sharp-edged fragments with remnant biostructure: pitted features, cross-hatching or thickenings Weak or no fluorescence
	Ph _{Br} Membranes	Light brown or grey non-cellular, angular sheets Non-fluorescent
Algae remains	Cuticles and other translucent fragments	Brown to colourless sheets with cellular or fibrous structures Strongly fluorescent
	A Prasinophycean phycomas, e.g. <i>Leiosphaeridia</i>	Discrete folded, circular or spinose entities Very strong fluorescence

	Acritarch cysts	
	Undifferentiated algal remains	Light brown to colourless tube-like filaments, yellow translucent non-cellular folded sheets Strong to very strong fluorescence
Sporomorphs	S Spores and Pollen	Miospores 30-100 μm Monosaccate pollen 150-300 μm Very strong fluorescence

Table 1: Palynofacies scheme based on observed organic particle properties under transmitted white and incident UV-light (after Combaz, 1980; Venkatachala, 1981; Batten, 1983, 1996; Highton et al., 1991; Tyson, 1995; Ercegovac and Kostić, 2006; Sebag et al., 2006, Stephenson et al., 2008).

Sporomorph Genera	Palaeobotanical Groups	Palaeoecological Groups
<i>Lycospora</i>	Arborescent lycopsids	Forest mire
<i>Densosporites</i>	Herbaceous lycopsids	
<i>Cristatisporites</i>	Various lycopsids	
<i>Camptotriletes</i>	Ferns	Non-forest mire
<i>Convolutispora</i>		
<i>Knoxisporites</i>		
<i>Punctatisporites</i>		
<i>Raistrickia</i>		
<i>Retusotriletes</i>		
<i>Savtrisporites</i>		
<i>Triquitrites</i>		
<i>Granulatisporites</i>		
<i>Leiotriletes</i>		
<i>Lophotriletes</i>		
<i>Microreticulatisporites</i>		
<i>Cyclogranisporites</i>		
<i>Verrocosisporites</i>		
<i>Calamospora</i>	Sphenopsids	
<i>Schulzospora</i>	Pteridospermae	
<i>Crassispora</i>	Sigillariaceae	Colonisers
<i>Florinites</i>	Cordaitaleans	Monosaccate pollen

Table 2: Observed sporomorph genera and related palaeoecological groups, modified after Stephenson et al. (2008), Davies and McLean (1996).

Sample*	MPA	Depth [m]	TOC [%]	$\delta^{13}\text{C}_{\text{org}}$ [‰]	Palynofacies [%]							
					AOM _{Gr}	AOM _{Br}	G	Ph _{Bl}	Ph _{Br}	A	S	
111	SSK4533	61598	14.76	4.9	-27.4	76.6	15.6	3.6	1.4	1.4	0.2	1.2
108	SSK4530	62605	15.50	6.5	-32.2	95.2	1.4	1.6	0.6	1.0	0.0	0.4
106	SSK4528	61599	16.75	4.5	-26.8	65.2	20.4	8.4	2.2	3.0	0.4	0.4
103	SSK4525	61600	18.18	0.3	-29.4	88.9	0.0	0.3	1.4	0.9	8.5	0.0
102	SSK4524	61601	18.77	3.1	-29.4	78.2	5.6	8.0	2.8	3.0	1.4	1.0
100	SSK4522	61602	19.17	5.2	-28.3	75.0	18.0	3.2	2.2	0.6	0.4	0.6
97	SSK4519	61115	20.62	5.4	-28.9	73.8	21.6	2.8	0.4	0.4	0.4	0.6
95	SSK4517	61114	20.95	4.4	-30.0	65.5	26.8	6.4	0.0	0.6	0.6	0.2
94	SSK4516	61113	21.30	4.0	-27.6	60.8	24.8	11.0	1.0	0.8	0.2	1.4
93	SSK4515	61112	21.98	3.2	-28.0	71.4	11.4	9.4	1.2	3.8	1.6	1.2
92	SSK4514	61111	22.36	3.3	-28.4	67.4	22.2	6.0	1.6	1.8	0.4	0.6
89	SSK4511	61110	23.41	2.9	-28.4	75.6	12.6	7.4	1.4	1.8	0.4	0.8
88	SSK4510	61109	25.30	4.2	-28.6	77.8	16.2	4.2	1.4	0.4	0.0	0.4
87	SSK4509	61108	25.75	5.1	-28.8	75.2	20.4	3.2	0.4	0.4	0.2	0.2
85	SSK4507	61107	26.59	4.8	-28.3	83.0	9.4	5.4	1.0	0.4	0.4	0.4
83	SSK4505	61603	27.21	4.1	-28.9	82.2	13.0	3.0	0.0	1.4	0.0	0.4
81	SSK4503	61106	27.76	3.6	-29.7	92.2	5.4	1.0	0.4	0.8	0.0	0.2
80	SSK4502	61105	28.42	2.6	-28.7	78.8	9.6	4.4	1.0	2.8	1.2	2.2
79	SSK4501	61104	28.68	4.5	-28.0	79.4	4.0	3.0	2.8	8.0	0.6	2.2
77	SSK4499	61103	29.04	4.5	-27.9	81.2	13.8	2.2	0.6	0.4	0.2	0.4
76	SSK4498	61102	29.75	3.7	-28.2	75.6	14.6	1.6	2.8	0.2	1.2	0.8
75	SSK4497	61101	30.13	4.1	-29.9	78.0	10.2	7.2	2.0	0.8	0.0	0.6
73	SSK4495	61100	30.62	3.3	-28.2	82.6	8.0	4.8	1.8	2.0	0.2	0.6
72	SSK4494	61099	31.02	3.8	-28.5	74.4	16.4	5.6	0.8	1.4	0.2	1.2
70	SSK4492	61098	32.20	(7.1)	(-20.5)	55.5	36.9	6.2	0.0	0.6	0.2	0.6
68	SSK4490	61097	33.01	(14.3)	(-18.1)	67.7	18.6	10.2	1.4	0.0	0.4	1.6
67	SSK4489	61096	33.48	3.5	-29.3	73.4	6.8	13.8	7.4	4.2	0.0	1.6
64	SSK4486	61095	34.30	1.3	-28.8	79.6	9.2	7.8	1.0	1.8	0.0	0.6
62	SSK4484	61094	34.72	2.1	-29.7	91.2	5.2	0.6	0.8	1.2	0.2	0.8
60	SSK4482	61093	35.30	2.0	-28.6	79.2	8.2	4.4	2.6	3.8	0.4	1.2
58	SSK4480	61604	35.84	1.1	-27.1	57.6	19.4	8.2	3.2	5.2	1.0	5.4
57	SSK4479	61092	36.09	1.7	-26.5	49.8	19.8	14.8	3.8	5.6	0.4	5.4
56	SSK4478	61091	36.75	1.4	-25.9	65.5	2.2	10.2	6.0	7.8	2.2	6.0
55	SSK4477	61605	37.08	(9.0)	(-7.7)	36.8	11.4	29.8	11.2	9.0	0.4	1.4
51	SSK4473	61606	38.11	2.4	-27.9	69.6	16.0	7.4	0.6	3.8	0.4	2.2
49	SSK4471	61090	38.73	(9.7)	(-23.4)	6.6	9.4	80.4	0.4	3.0	0.0	0.2
48	SSK4470	61607	38.95	1.2	-26.5	63.6	19.2	11.2	0.2	3.8	0.8	1.2

46	SSK4468	61608	39.42	3.4	-26.2	57.7	21.0	7.8	2.4	9.0	0.2	1.8
43	SSK4465	61609	40.00	2.6	-25.9	33.0	14.4	40.2	4.2	7.2	0.2	0.8
42	SSK4464	61610	40.60	3.0	-28.9	74.4	20.2	1.6	1.0	0.6	0.2	1.8
39	SSK4461	61611	41.72	3.7	-27.0	49.2	20.2	17.4	4.0	3.4	1.0	4.8
35	SSK4457	61612	42.70	1.9	-28.4	73.6	14.8	4.8	2.0	2.8	0.2	1.8
33	SSK4455	61613	43.41	1.6	-26.8	51.8	24.8	16.6	1.8	4.2	0.0	0.4
28	SSK4450	61614	44.78	1.7	-27.0	58.2	25.0	5.8	4.2	5.0	0.6	1.2
27	SSK4407	61615	45.01	2.6	-28.7	53.2	16.4	13.2	2.4	11.8	0.2	2.8
26	SSK4406	61616	45.22	1.7	-25.1	11.0	16.0	31.2	21.2	17.6	0.2	2.8
24	SSK4404	61617	46.25	0.9	-27.4	34.8	49.8	10.4	1.8	1.6	0.2	0.6
23	SSK4403	62606	46.78	2.1	-25.0	57.4	25.6	10.4	0.8	3.8	0.2	1.8
22	SSK4402	61618	47.30	2.3	-28.3	92.0	11.8	3.4	1.4	1.0	0.0	0.4
19	SSK4399	61619	48.20	3.6	-29.0	77.8	14.8	3.0	1.6	1.8	0.0	1.0
17	SSK4397	61620	49.05	2.5	-29.0	79.2	15.0	0.6	0.6	1.4	1.0	2.0
15	SSK4395	61621	49.70	2.6	-29.0	77.4	15.6	2.6	0.8	2.0	0.6	1.0
13	SSK4393	61622	50.45	2.0	-28.8	60.8	25.0	6.4	1.2	3.8	0.4	2.4
11	SSK4391	61623	51.14	2.1	-28.0	80.2	10.0	4.0	1.6	3.0	0.0	1.2
9	SSK4389	61624	51.95	2.9	-28.4	83.4	8.0	2.2	1.4	2.0	1.2	1.8
7	SSK4387	61625	52.64	6.4	-28.0	85.0	10.2	2.8	0.6	0.6	0.0	0.8
4	SSK4384	61626	53.28	1.4	-26.6	56.0	19.0	9.0	3.4	9.6	0.2	3.0
1	SSK4381	61627	55.18	2.8	-25.6	17.4	5.8	37.2	27.8	10.8	0.4	0.6

Table 3: TOC (obtained from EA), bulk $\delta^{13}\text{C}_{\text{org}}$ and palynofacies composition data for all samples used for palynological processing. Data from samples containing residual inorganic carbon (dolomite or siderite) are shown in brackets. *British Geological Survey reference number.

Sample*	Depth [m]	Sample type	Comments	$\delta^{13}\text{C}_{\text{org}}$ [‰]
SSK4522	19.17	Organic residue 10-106 μm	Predominance of AOM _{Gr} with inclusions	-27.8
SSK4505	27.21	Organic residue 180-300 μm	Mainly AOM _{Gr} , some with large inclusions	-28.9
SSK4503	27.76	Organic residue 180-355 μm	Large dense AOM _{Gr} particles, some with inclusions	-28.3
SSK4486	34.30	Organic residue 10-150 μm	Dominant small translucent AOM _{Gr}	-28.5
SSK4402	47.30	Organic residue 106-250 μm	Dominant AOM _{Gr} , some with inclusions	-28.7
SSK4391	51.14	Organic residue 10-106 μm	AOM _{Gr} dominant, with few miospores	-29.0
SSK13397	15.32	Thin leaf material		-24.0
SSK13396	22.58	Coalified woody material		-27.1
SSK13395	26.24	Coalified woody material		-26.4
SSK13393	39.25	Coalified woody material		-24.9
SSK13391	44.00	Coalified woody material		-26.4
SSK4401	47.51	Coalified woody material	Separated from bulk sample	-25.1
SSK13390	50.30	Thin leaf material		-26.3
SSK13389	53.67	Mixture of wood and leaves		-25.7
SSK4381	55.18	Coalified woody material	Separated from bulk sample	-25.1

Table 4: $\delta^{13}\text{C}_{\text{org}}$ data of isolated OM fractions - AOM and plant material. *British Geological Survey reference number.

Lithofacies	1	2	3	4a	4b	4c	5	6	7
No. of samples	20	1	9	4	12	1	6	4	1
AOM _{Gr}	75.3±7.7	88.9	75.1±10.6	74.2±15.7	69.8±11.0	49.2	41.7±17.2	41.5±20.4	6.6
AOM _{Br}	14.5±6.8	-	15.0±7.6	14.2±6.4	17.2±12.3	20.2	19.3±5.2	16.1±8.0	14.6
G	5.7±3.3	0.3	5.2±3.7	4.6±5.8	5.2±3.3	17.4	17.0±10.8	26.3±14.5	80.4
Ph _{Bl}	1.6±1.7	1.4	1.1±0.9	1.5±0.7	1.9±1.1	4.0	8.3±7.4	8.5±13.0	0.4
Ph _{Br}	1.5±1.3	0.9	1.5±1.3	3.9±5.3	3.2±2.5	3.4	9.7±5.0	6.5±3.2	3.0
S	0.9±0.6	-	1.1±0.8	1.6±0.9	1.7±1.4	4.8	3.4±1.9	0.9±0.3	0.2
A	0.4±0.4	8.5	0.4±0.9	0.2±0.2	0.5±0.4	1.0	0.5±0.5	0.4±0.3	-

Table 5: Means and standard deviations of palynofacies groups [%] according to lithofacies.

Means are also shown in Figure 8.

Sample*	Depth [m]	TOC [%]	AOM _{Gr}	AOM _{Br}	G	Ph _{Bl}	Ph _{Br}	S [10 ³ /g]	A [10 ³ /g eq]	Total [10 ⁶ /g eq]
111 SSK4533	14.76	4.9	3.105	0.632	0.146	0.057	0.057	48.6	8.1	4.053
108 SSK4530	15.50	6.5	4.627	0.068	0.078	0.029	0.039	19.4	0.0	4.860
106 SSK4528	16.75	4.5	7.446	2.330	0.959	0.251	0.343	45.7	45.7	11.420
95 SSK4517	20.95	4.4	8.148	3.334	0.796	0.000	0.075	24.9	74.6	12.452
93 SSK4515	21.98	3.2	5.119	0.817	0.674	0.086	0.272	114.7	86.0	7.170
87 SSK4509	25.75	5.1	7.971	2.162	0.339	0.042	0.042	21.2	21.2	10.600
81 SSK4503	27.76	3.6	8.261	0.484	0.108	0.036	0.054	17.9	0.0	8.960
79 SSK4501	28.68	4.5	3.948	0.199	0.379	0.140	0.170	109.7	29.9	4.975
75 SSK4497	30.13	4.1	7.935	1.038	0.732	0.203	0.081	61.0	0.0	10.051
67 SSK4489	33.48	3.9	3.926	0.401	0.714	0.436	0.189	94.3	0.0	5.860
57 SSK4479	36.09	1.7	0.972	0.387	0.289	0.074	0.109	105.4	7.8	1.944
43 SSK4465	40.00	2.6	0.851	0.372	1.037	0.108	0.186	20.6	5.2	2.580
39 SSK4461	41.72	3.7	2.839	1.166	1.004	0.231	0.196	277.0	57.7	5.771
23 SSK4403	46.78	2.1	6.860	3.059	1.243	0.096	0.454	215.1	23.9	11.951
13 SSK4393	50.45	2.0	2.605	1.071	0.274	0.051	0.162	102.8	17.1	4.285
7 SSK4387	52.64	6.4	4.242	0.509	0.140	0.030	0.030	39.9	0.0	4.990

Table 6: Concentrations of palynofacies types, calculated from the observed concentration of sporomorphs (highlighted). TOC data is derived from elemental analyser. *British Geological Survey reference number.

Sample*	Depth [m]	TOC [%]	S1 [mg/g]	S2 [mg/g]	S3 [mg/g]	T _{max} [°C]	HI	OI	
							[mg HC/ g TOC]	[mg CO ₂ / g TOC]	
111	SSK4533	14.76	2.73	0.59	12.01	0.35	426	440	13
107	SSK4529	16.57	4.11	1.90	19.90	0.47	425	484	11
104	SSK4526	18.05	4.18	0.77	11.41	0.55	424	273	13
103	SSK4525	18.18	3.84	2.85	17.82	1.01	424	464	26
102	SSK4520	20.48	2.95	0.76	10.12	0.86	424	343	29
100	SSK4513	22.70	1.80	0.37	5.94	0.31	425	330	17
89	SSK4511	23.41	2.09	0.38	8.14	0.40	430	389	19
84	SSK4506	26.90	3.31	1.87	14.12	0.70	424	427	21
80	SSK4502	28.42	2.05	0.34	7.44	0.29	439	363	14
77	SSK4499	29.04	3.26	0.67	16.22	0.36	426	498	11
74	SSK4496	30.24	2.95	0.37	9.43	0.46	427	320	16
66	SSK4488	33.66	2.93	0.39	5.69	0.87	428	194	30
63	SSK4485	34.60	1.13	0.08	2.95	0.13	440	261	12
61	SSK4483	34.82	1.38	0.09	5.41	0.12	440	392	9
58	SSK4480	35.59	0.72	0.06	0.56	0.22	432	78	31
51	SSK4473	38.11	1.46	0.35	2.55	0.50	436	175	34
48	SSK4470	38.96	0.71	0.16	1.32	0.13	438	186	18
43	SSK4465	40.00	1.35	0.22	2.09	0.22	440	155	16
42	SSK4464	40.60	2.08	0.28	8.06	0.44	437	388	21
39	SSK4461	41.72	2.08	0.20	2.04	0.35	426	98	17
36	SSK4458	42.60	0.91	0.06	1.26	0.19	434	138	21
33	SSK4455	43.41	1.12	0.13	2.81	0.17	439	251	15
30	SSK4452	44.17	1.81	0.11	8.35	0.22	442	461	12
29	SSK4451	44.37	1.23	0.12	3.45	0.35	438	280	28
27	SSK4407	45.01	2.07	1.56	7.76	1.20	438	375	58
26	SSK4406	45.22	1.10	0.11	1.06	0.32	440	96	29
21	SSK4401	47.51	4.84	2.51	19.49	0.99	434	403	20
20	SSK4400	47.86	1.91	0.14	8.65	0.27	440	453	14
14	SSK4394	50.10	0.25	0.05	0.32	0.14	439	128	56
8	SSK4388	52.28	1.94	0.82	4.86	1.42	365	251	73
7	SSK4387	52.64	4.59	0.74	14.02	0.92	423	305	20
1	SSK4381	55.18	1.90	0.54	3.00	0.26	437	158	14

Table 7: Rock-Eval Pyrolysis parameters. *British Geological Survey reference number.

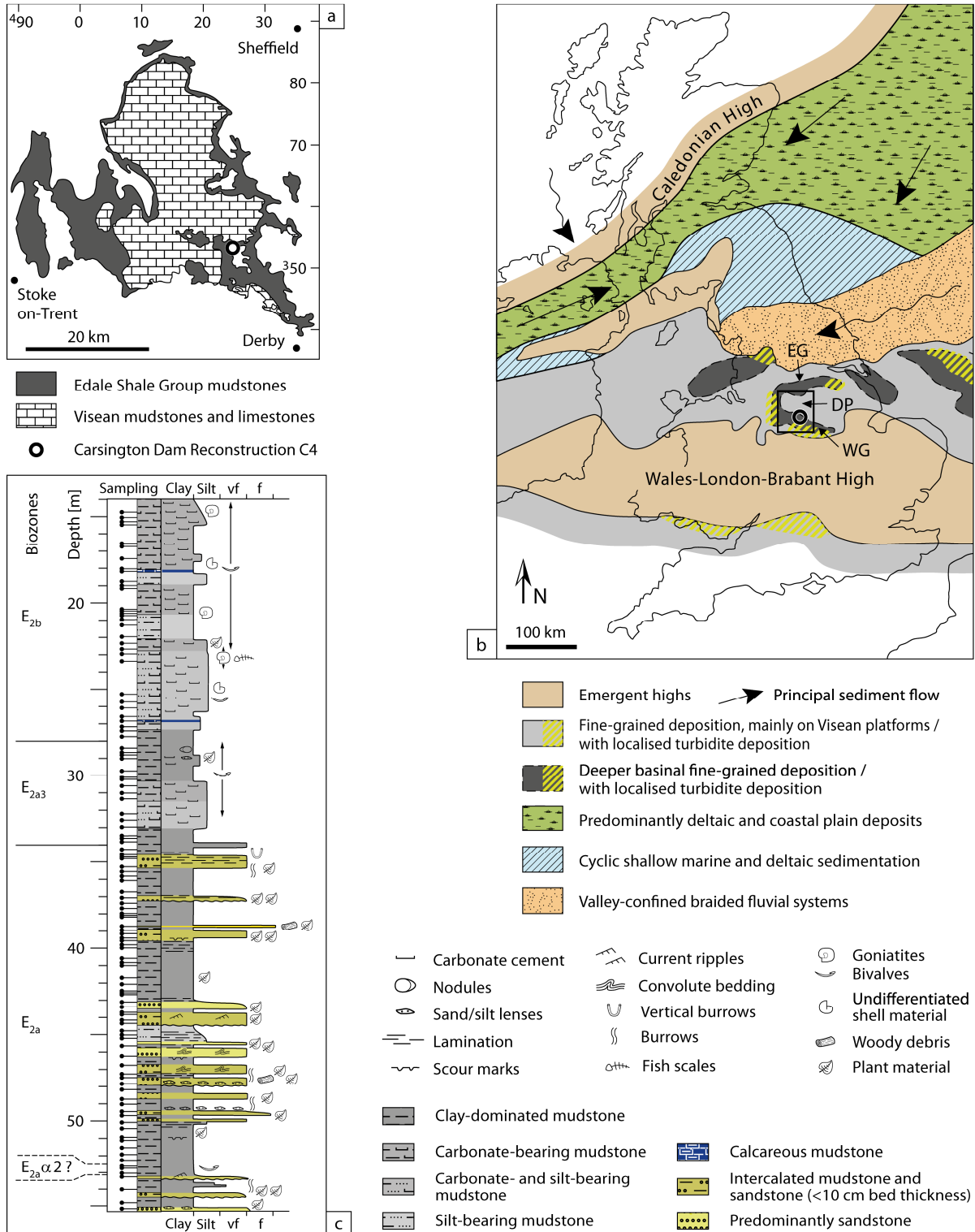


Figure 1

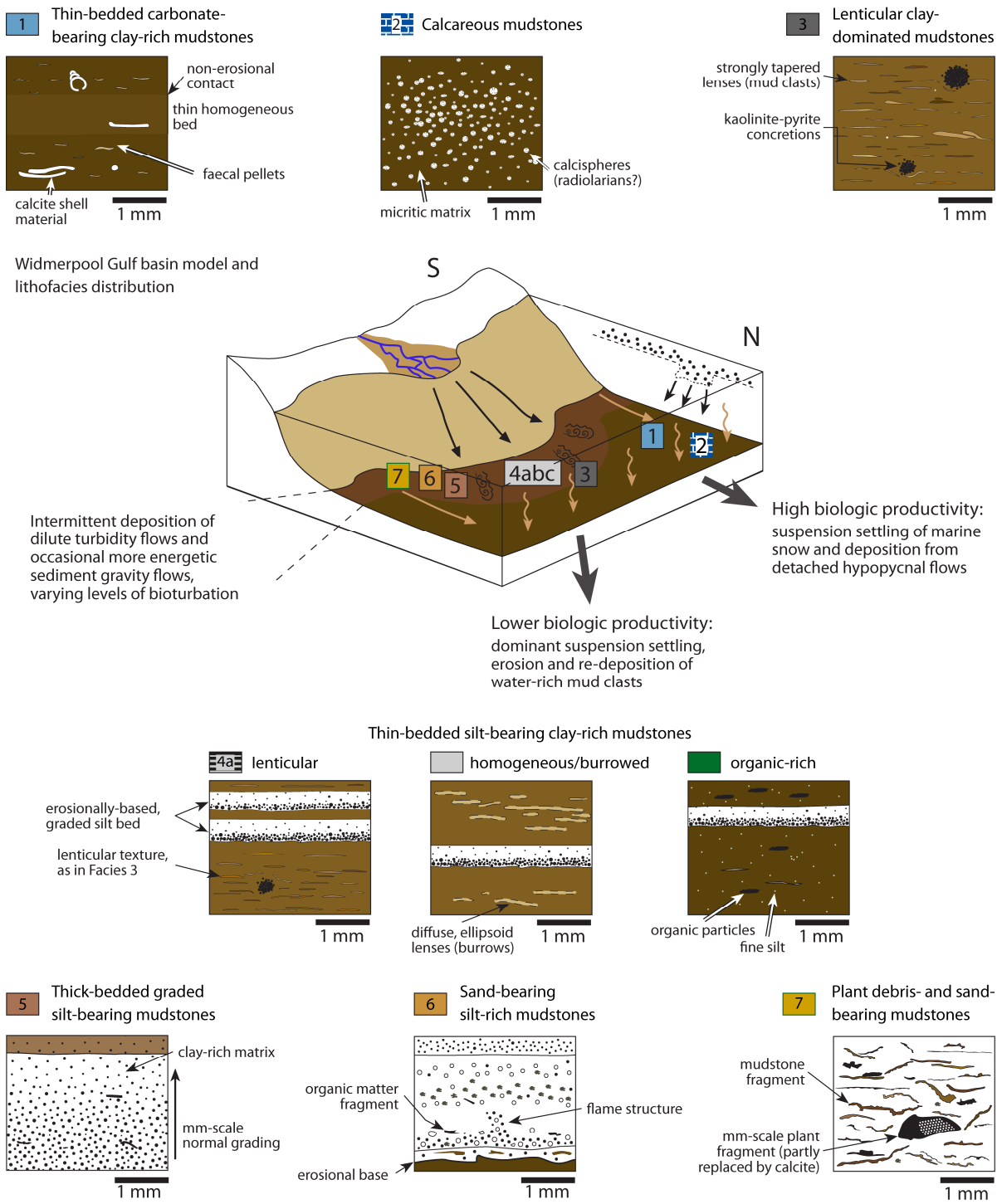


Figure 2

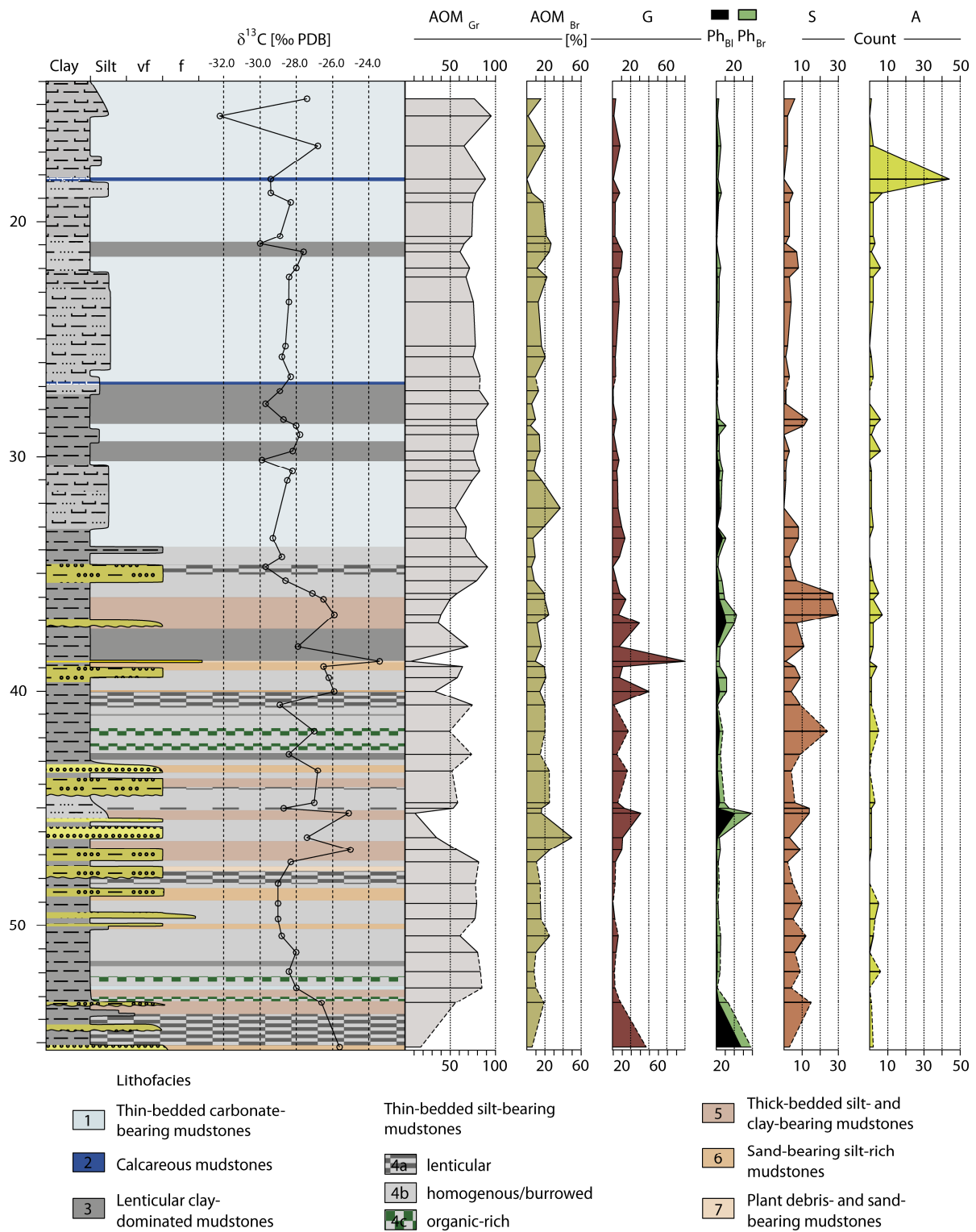


Figure 3

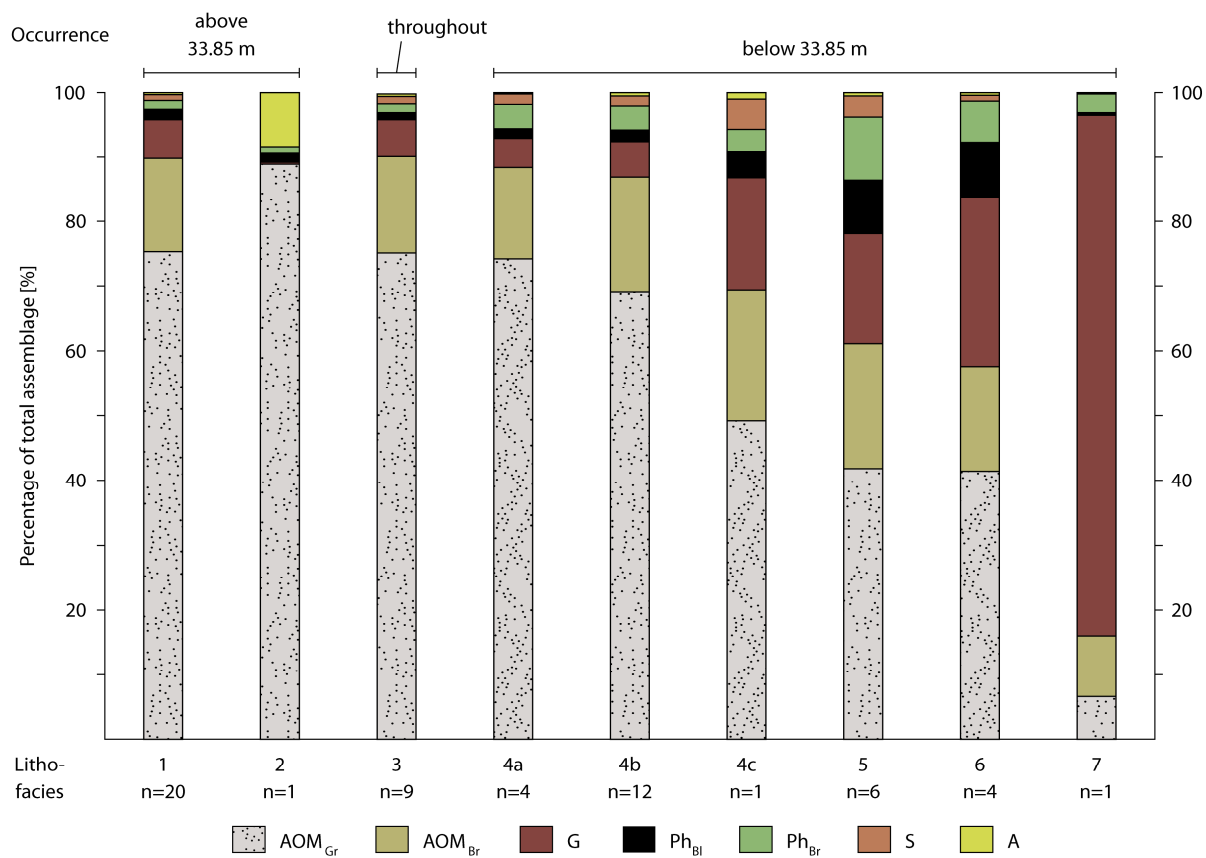


Figure 4

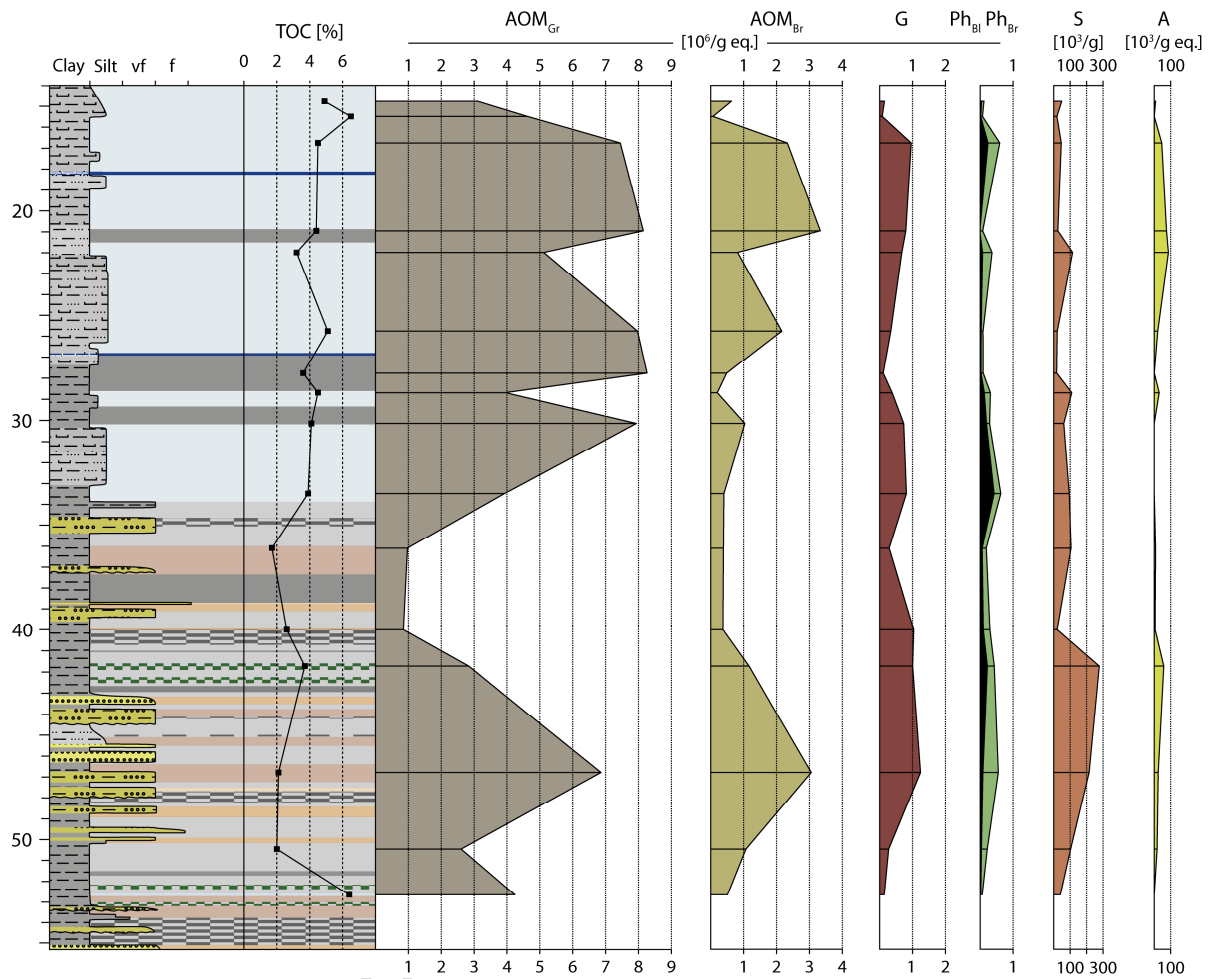


Figure 5

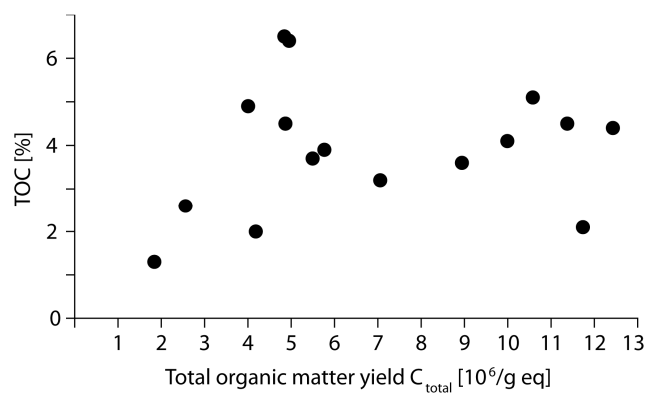


Figure 6

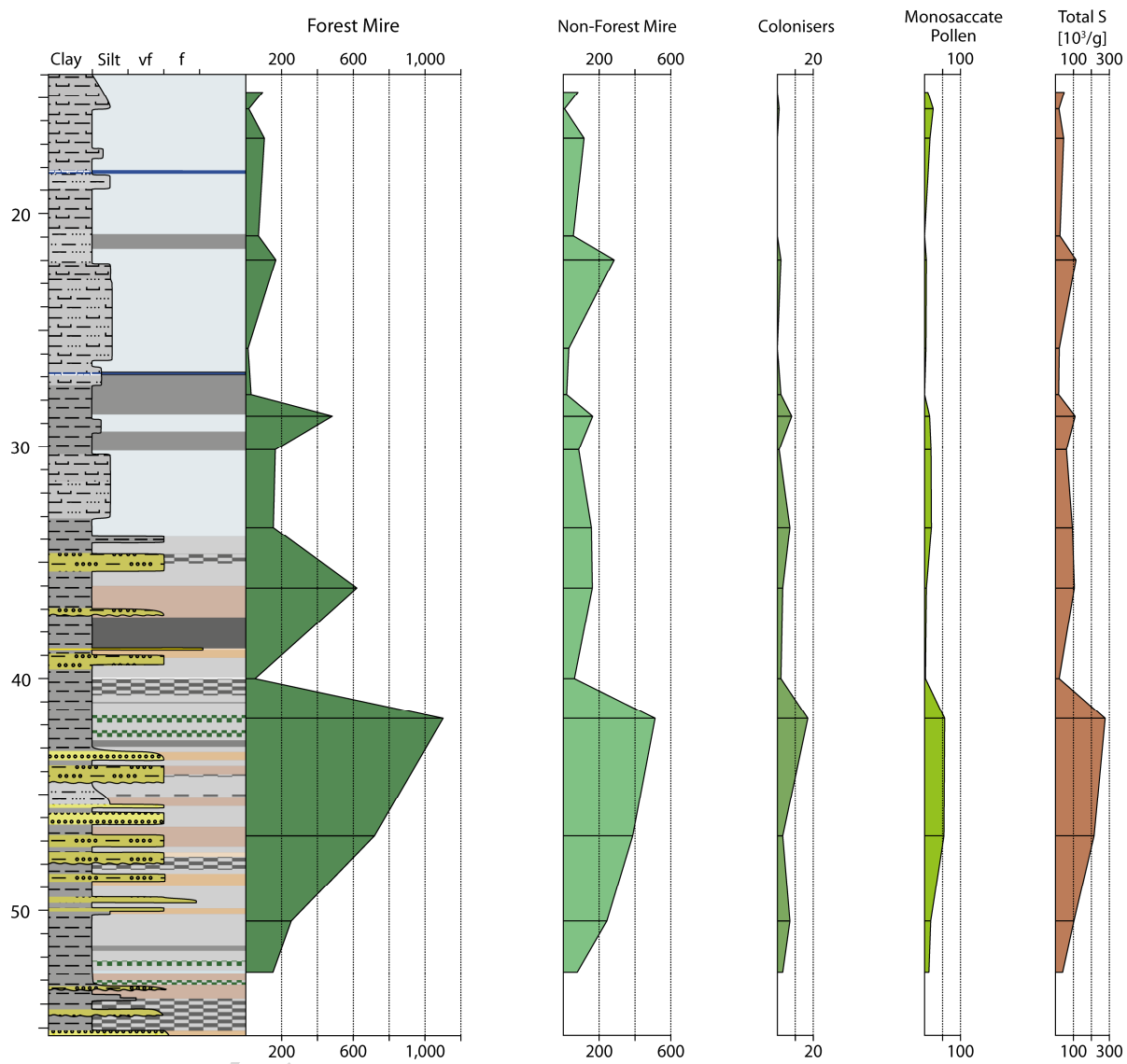


Figure 7

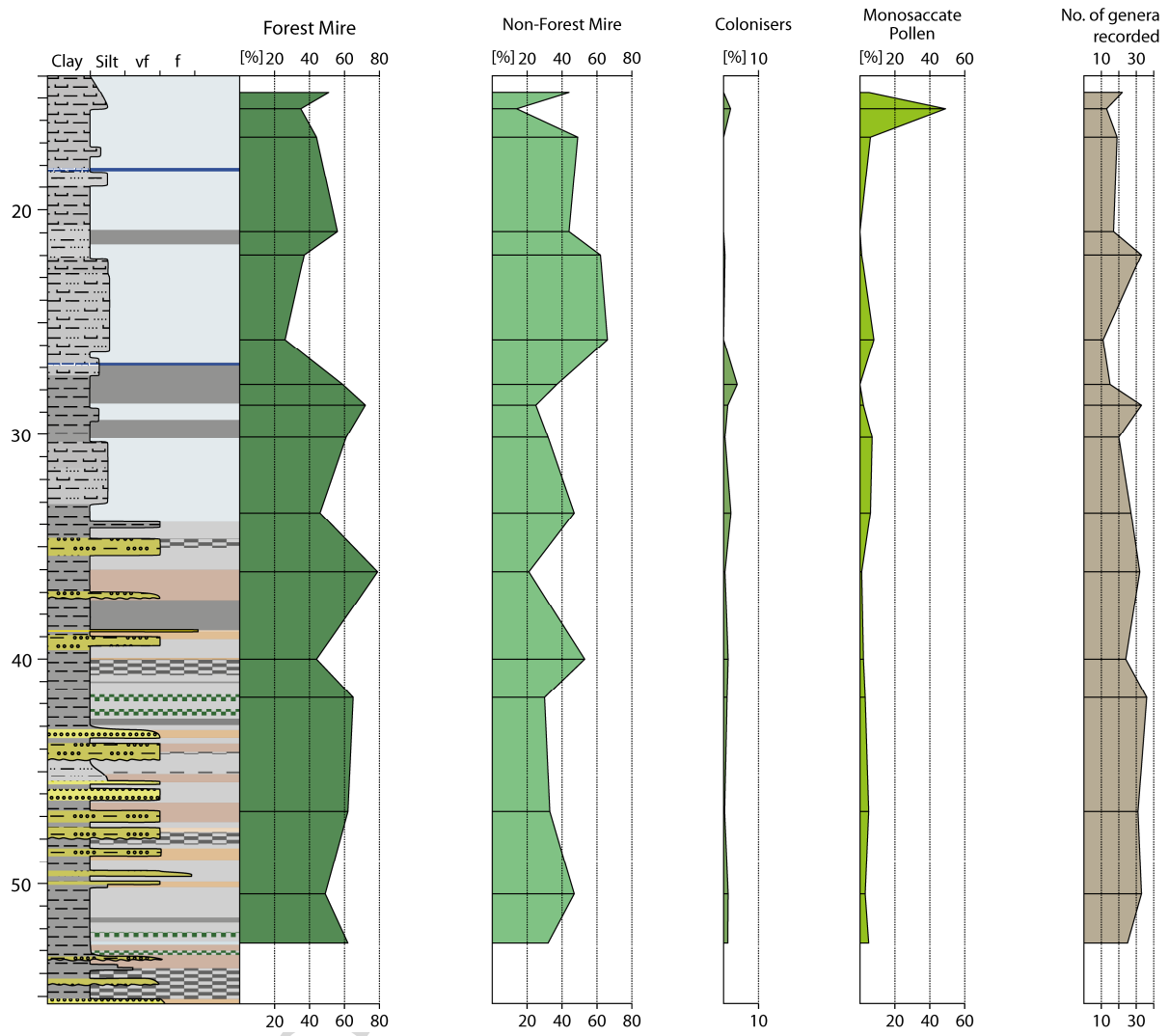


Figure 8

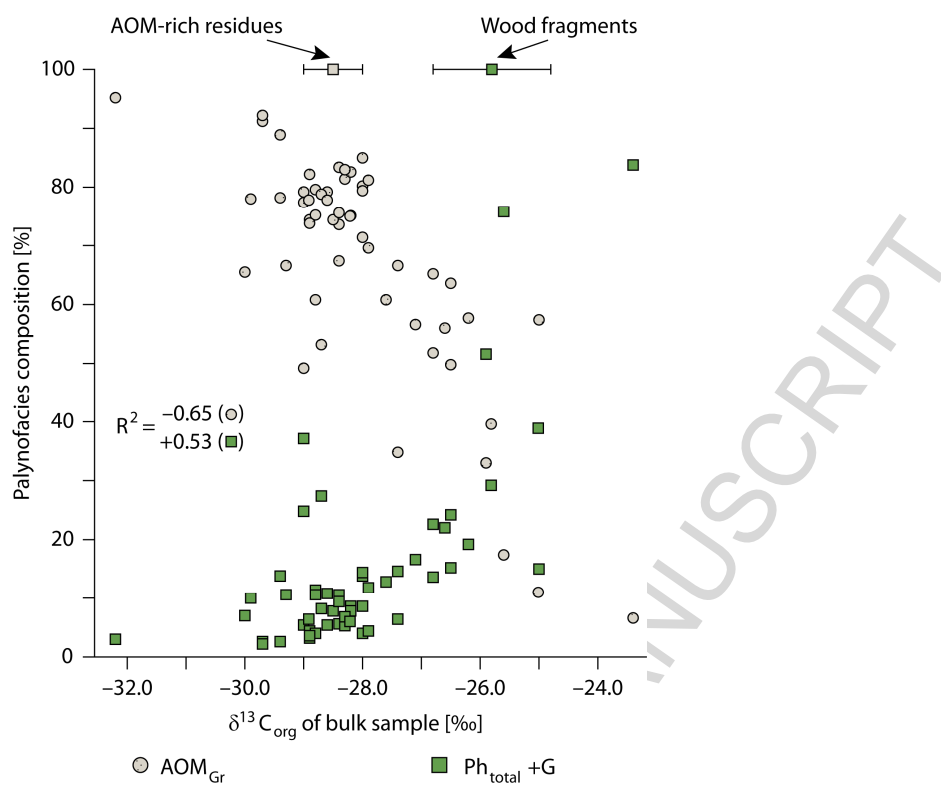
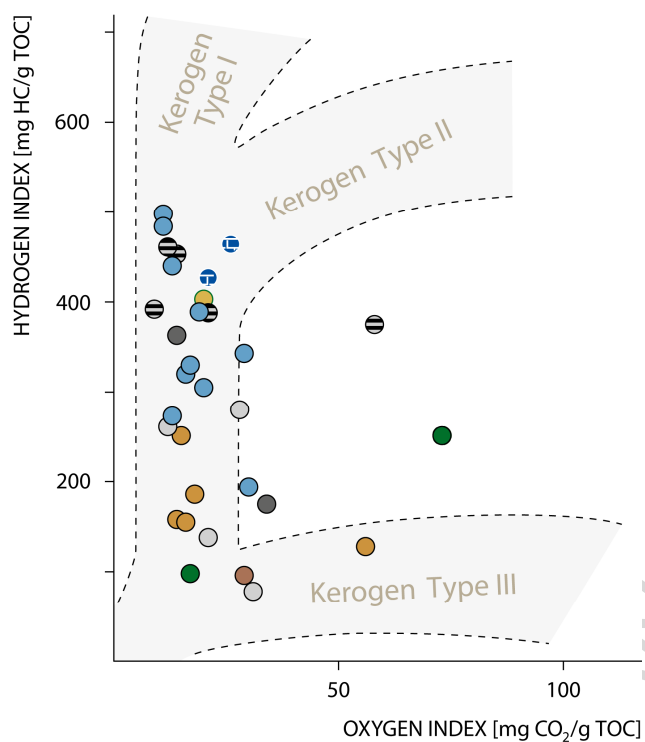


Figure 9



- 1 Thin-bedded carbonate-bearing mudstones
- 2 Calcareous mudstones
- 3 Lenticular clay-dominated mudstones
- 4 Thin-bedded silt-bearing mudstones
 - ⊖ a lenticular
 - b homogenous
 - c organic-rich
- 5 Thick-bedded silt-bearing mudstones
- 6 Sand-bearing silt-rich mudstones
- 7 Plant debris- and sand-bearing mudstones

Figure 10

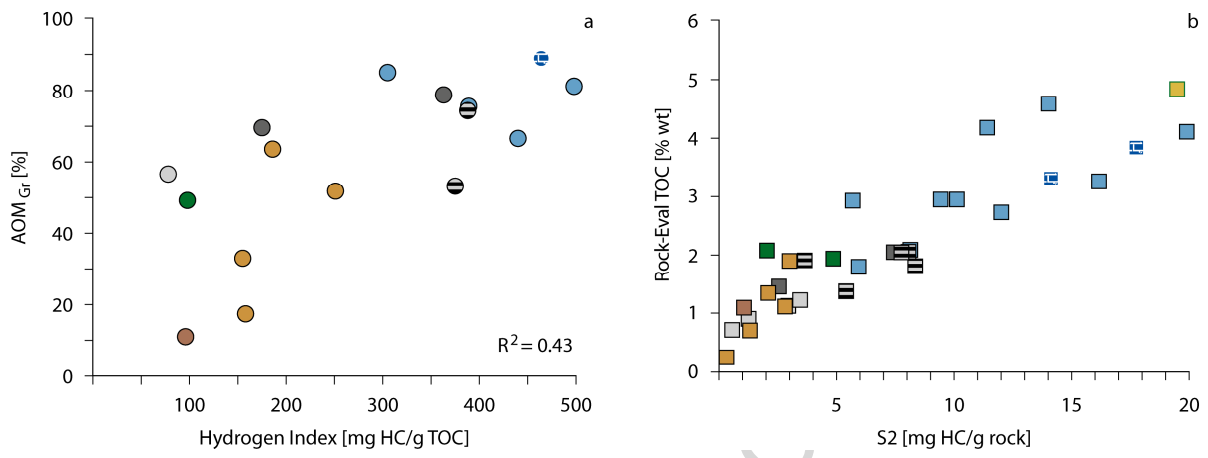


Figure 11

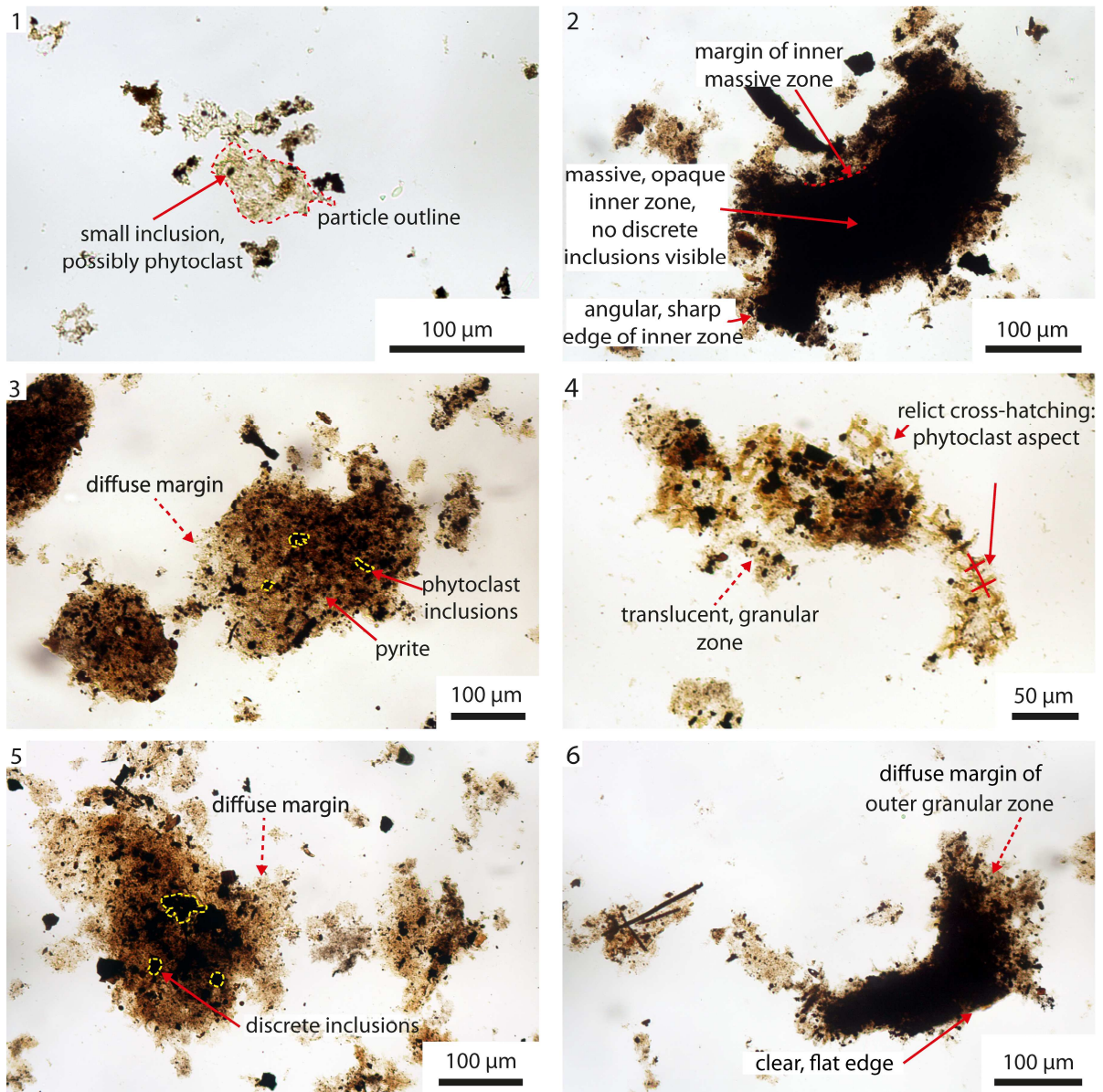


Plate I

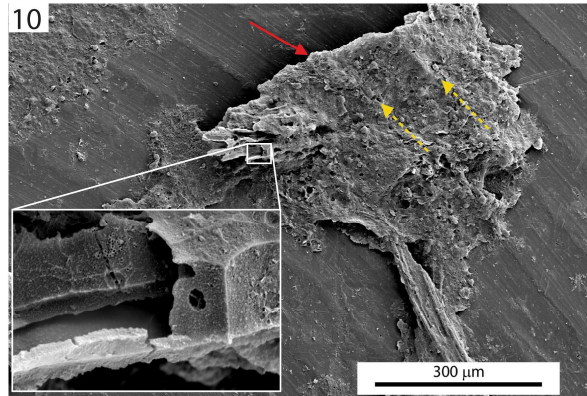
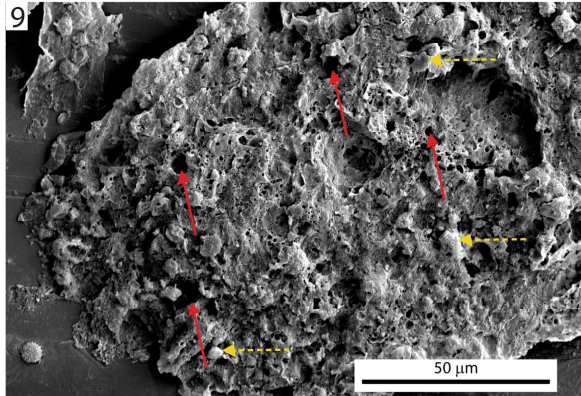
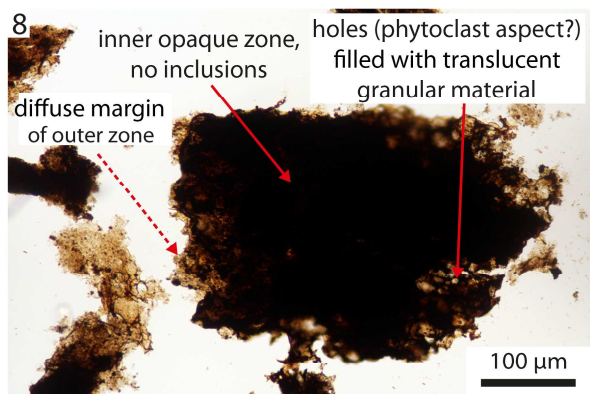
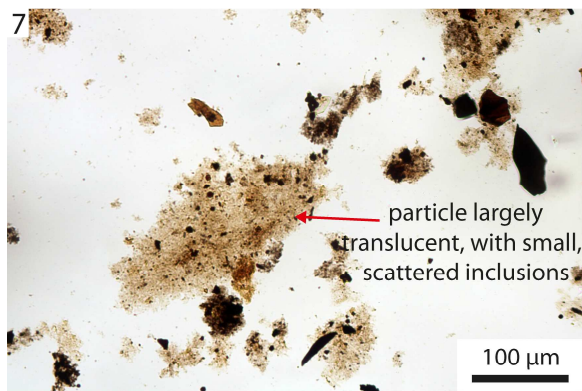


Plate I

ACCEPTED

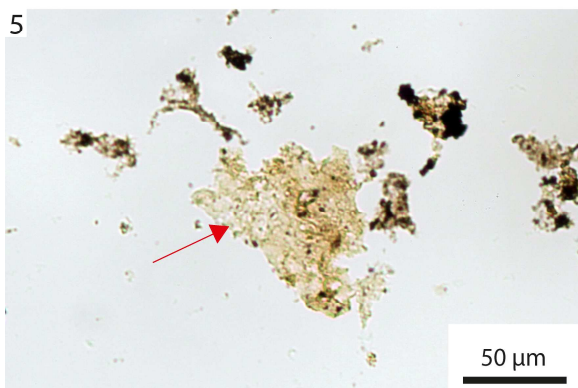
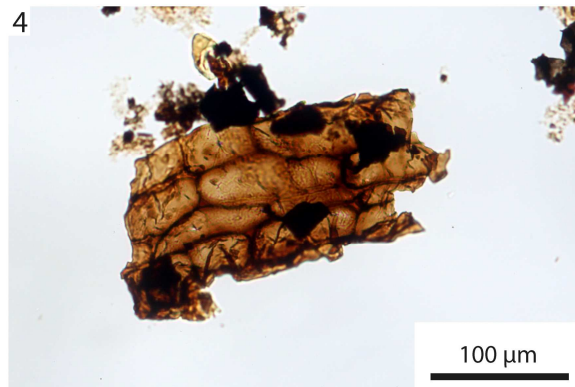
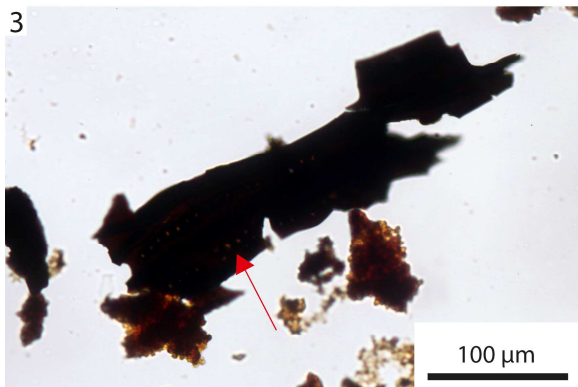
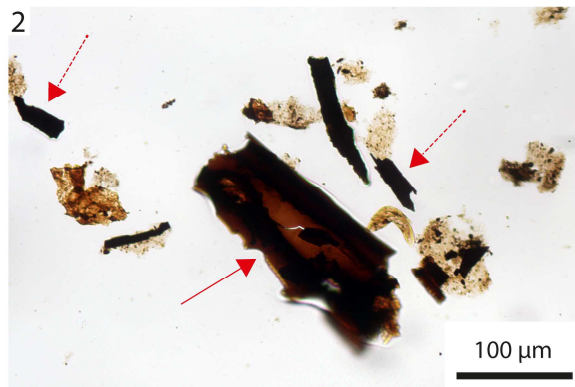
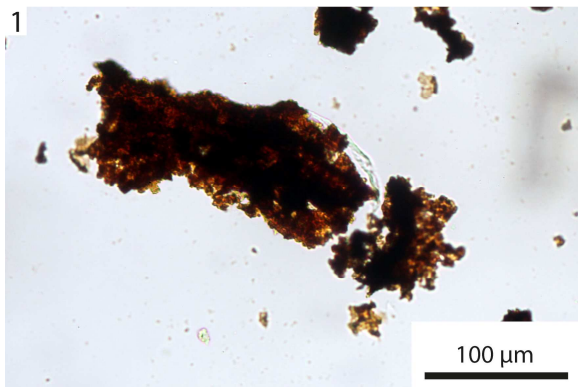
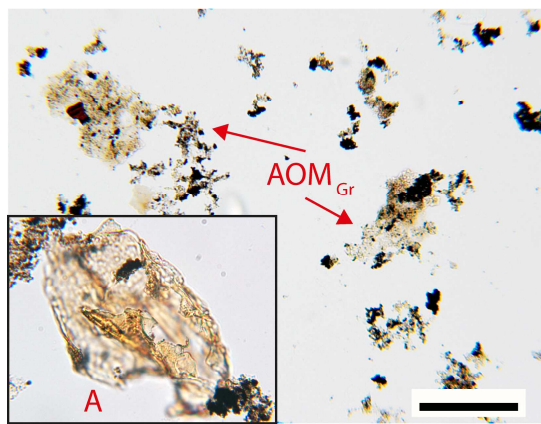
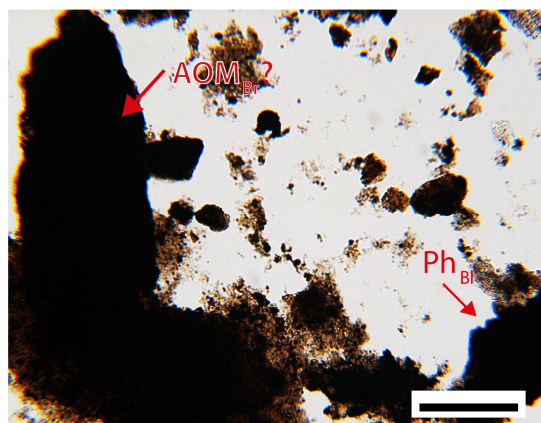
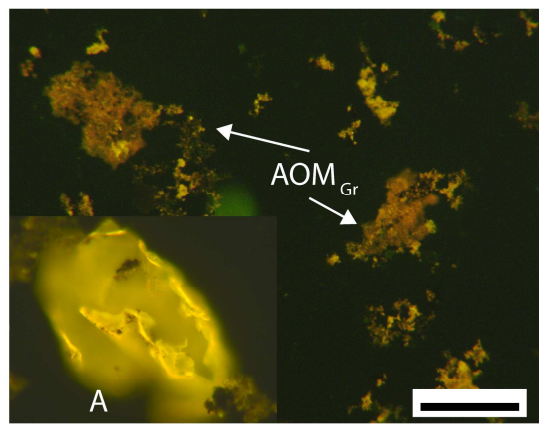


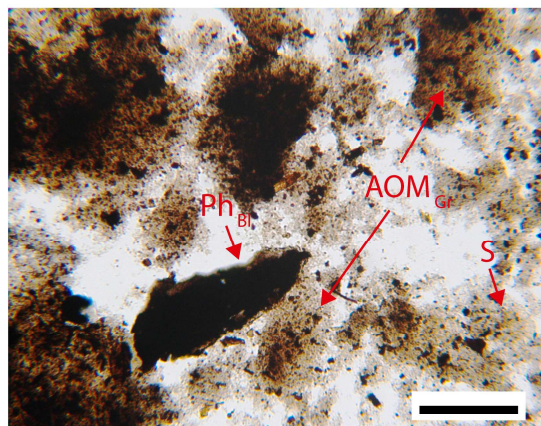
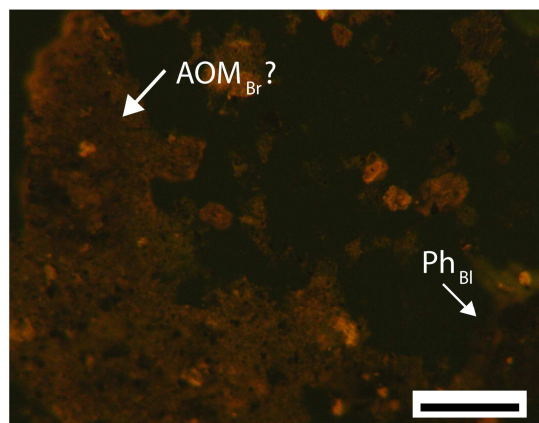
Plate II



1



2



3

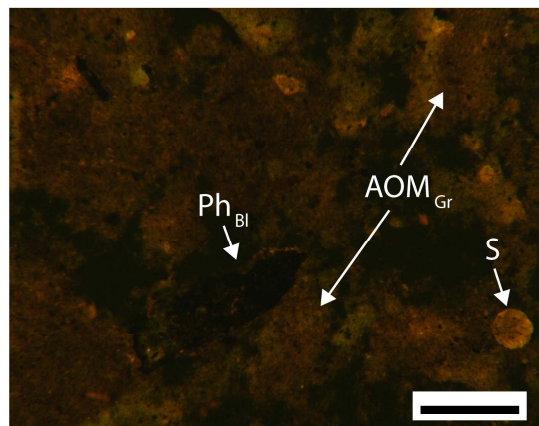
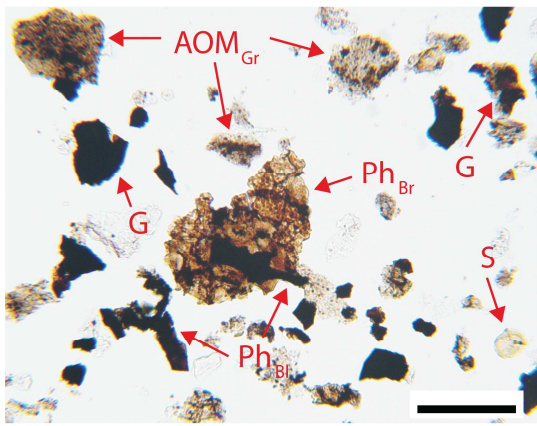


Plate III



4

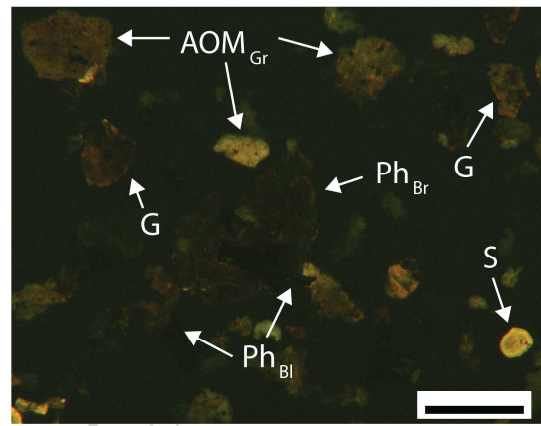


Plate IV

ACCEPTED MANUSCRIPT

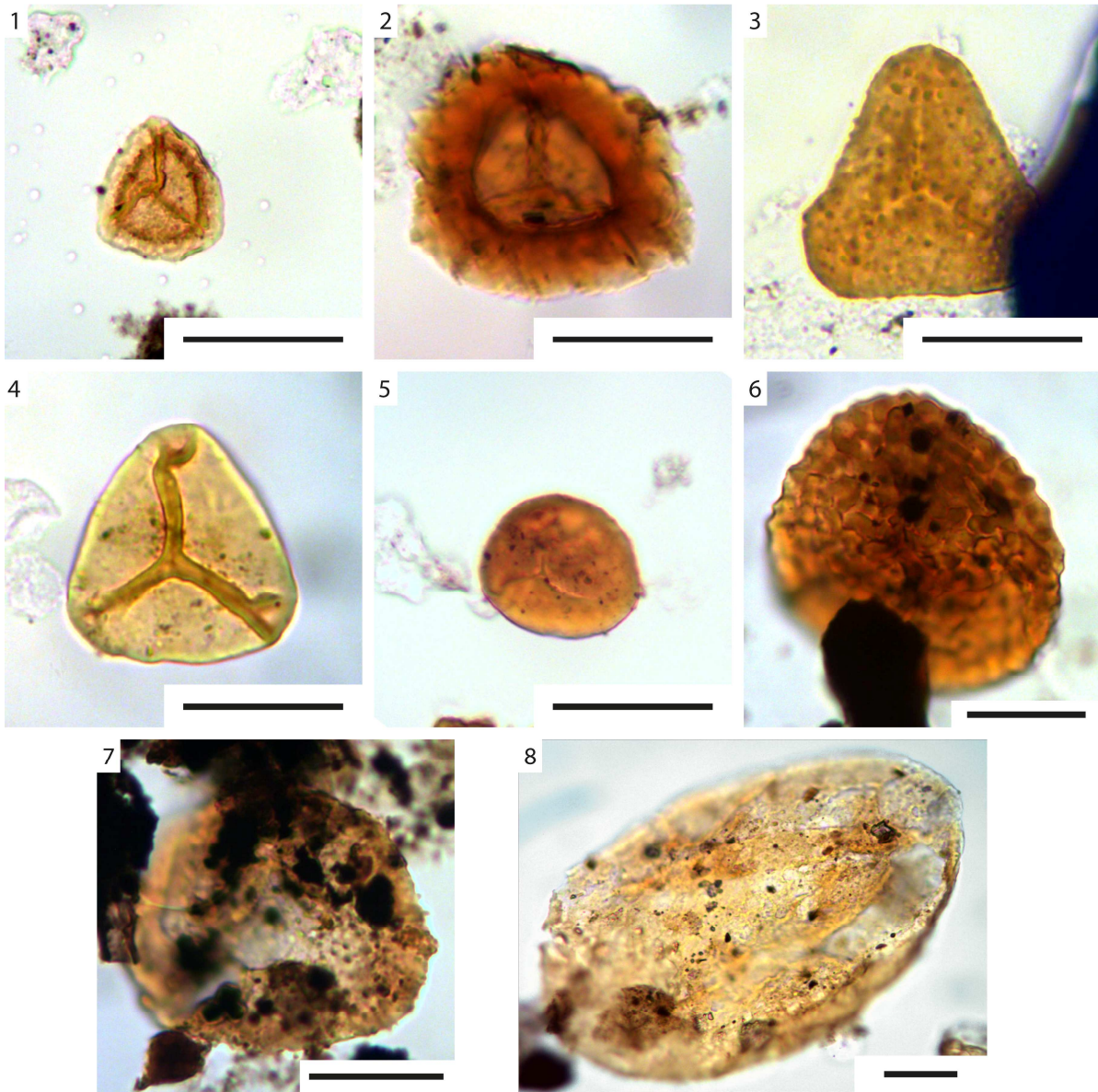


Plate V